AD-785 412

INFRARED RADIATION FROM H20, CO2 OR NH3 COLLISIONALLY EXCITED BY N2, O, OR ARGON

Michael G. Dunn, et al

Calspan Corporation

Prepared for:

Air Force Rocket Propulsion Laboratory
Defense Advanced Research Projects Agency

July 1974

DISTRIBUTED BY:

NTIS

National Technical Information Service
U. S. DEPARTMENT OF COMMERCE
5285 Port Royal Road, Springfield Va. 22151

AD785412

AFRPL-TR-74-30

INFRARED RADIATION FROM H_2O, CO_2, OR NH_3 COLLISIONALLY EXCITED BY N_2, O, OR ARGON

Final Report

Michael G. Dunn
George T. Skinner
Charles E. Treanor

CALSPAN CORPORATION
Buffalo, New York 14221

JULY 1974

APPROVED FOR PUBLIC RELEASE;
DISTRIBUTION UNLIMITED

SPONSORED BY:

STRATEGIC TECHNOLOGY OFFICE
DEFENSE ADVANCED RESEARCH PROJECTS AGENCY
DARPA ORDER 1867

DDC
RECEIVED
SEP
B

PREPARED FOR:

AIR FORCE ROCKET PROPULSION LABORATORY
DIRECTOR OF SCIENCE AND TECHNOLOGY
AIR FORCE SYSTEMS COMMAND
UNITED STATES AIR FORCE
EDWARDS, CALIFORNIA 93523

Reproduced by
NATIONAL TECHNICAL
INFORMATION SERVICE
U S Department of Commerce
Springfield VA 22151

78

This technical report has been reviewed and is approved.

FOR THE COMMANDER

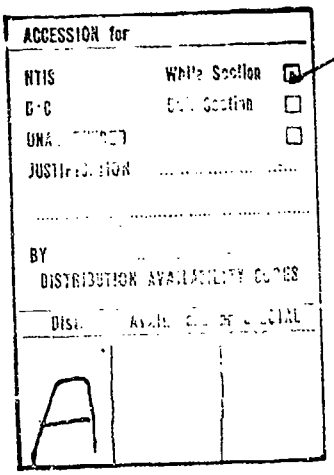

Paul J. Daily, Colonel, USAF
Chief, Technology Division

NOTICES

When U.S. Government drawings, specifications, or other data are used for any purpose than a definitely related Government procurement operation, the Government thereby incurs no responsibility, nor any obligation whatsoever, and the fact that the Government may have formulated, furnished or in any way supplied the said drawings, specifications, or other data, is not to be regarded by implication or otherwise, or in any manner as licensing the holder or any other person or corporation, or conveying any rights or permission to manufacture, use, or sell any patented invention that may in any way be related thereto.

REPORT DOCUMENTATION PAGE

READ INSTRUCTIONS BEFORE COMPLETING FORM

1. REPORT NUMBER: AFRPL-TR-74-30	2. GOVT ACCESSION NO.
3. RECIPIENT'S CATALOG NUMBER	
4. TITLE (and Subtitle): Infrared Radiation from H_2O, CO_2 or NH_3 Collisionally Excited by N_2, O or Argon	5. TYPE OF REPORT & PERIOD COVERED: Final Report, April 1972 - January 1974
	6. PERFORMING ORG. REPORT NUMBER
7. AUTHOR(s): Michael G. Dunn, George T. Skinner and Charles E. Treanor	8. CONTRACT OR GRANT NUMBER(s): F04611-72-C-0035
9. PERFORMING ORGANIZATION NAME AND ADDRESS: Calspan Corporation, P.O. Box 235, Buffalo, New York 14221	10. PROGRAM ELEMENT, PROJECT, TASK AREA & WORK UNIT NUMBERS: DARPA Order 1857
11. CONTROLLING OFFICE NAME AND ADDRESS: Strategic Technology Office, Defense Advanced Research Projects Agency, 1400 Wilson Blvd., Arlington VA	12. REPORT DATE: July 1974 13. NUMBER OF PAGES: 78
14. MONITORING AGENCY NAME & ADDRESS (if different from Controlling Office): Air Force Rocket Propulsion Laboratory/DYSP, Edwards, California 93523	15. SECURITY CLASS. (of this report): Unclassified 15a. DECLASSIFICATION/DOWNGRADING SCHEDULE: N/A

16. DISTRIBUTION STATEMENT (of this Report)
APPROVED FOR PUBLIC RELEASE; DISTRIBUTION UNLIMITED

17. DISTRIBUTION STATEMENT (of the abstract entered in Block 20, if different from Report)

18. SUPPLEMENTARY NOTES

19. KEY WORDS (Continue on reverse side if necessary and identify by block number)
1) Collisionally induced Infrared Radiation
2) Excitation cross sections for N_2 - H_2O, N_2 - CO_2, N_2 - NH_3, O - H_2O and Ar - H_2O
3) Vibrational and Rotational Infrared Radiation

20. ABSTRACT (Continue on reverse side if necessary and identify by block number)

Results are reported of an experimental study to elicit the spectral infrared radiative properties of H_2O, CO_2 or NH_3 molecules that have been involved in a single high-energy collision with N_2, O, or Argon. A pressure-driven reflected-shock tunnel was used to produce a 5.8 Km/sec supply of N_2 molecules or a 4.3 Km/sec supply of O atoms or a 5.4 Km/sec supply of argon that subsequently impacted the target molecules. Experimental values of σ_*/τ (excitation cross section/radiative lifetime)

20.
are presented for the wavelength regions 2.5 to 3.1μm, 5.7 to 7.5μm, 8.3 to 9.2μm, 9.1 to 10.3μm, 10.6 to 11.6μm, 11.1 to 14.0μm, and 8.3 to 14.0μm for the N_2-H_2O collisions. Values of σ_*/τ are also presented for the N_2-CO_2 collisions in the wavelength regions 4.28 to 4.34μm, 8.3 to 9.2μm, 9.1 to 10.3μm, 10.6 to 11.6μm, and 8.3 to 14.0μm. In addition, values of σ_*/τ are reported for the N_2-NH_3 interaction in the wavelength intervals 8.3 to 9.2μm, 10.6 to 11.6μm, and 8.3 to 14.0μm. Experimental values of σ_*/τ are also presented for the O-H_2O interaction in the wavelength intervals 2.46 to 3.13μm, 5.67 to 7.45μm and 11.1 to 14.0μm. A value of σ_*/τ is given for Ar-H_2O collisions at 5.4 Km/sec in the wavelength interval 5.67 to 7.45. These experimental values of σ_*/τ are compared with theoretical calculations of the effective values of σ_*/τ for radiation in the given wavelength intervals. Using available values of the radiative lifetimes, values for σ_* were obtained.

PREFACE

This final report documents an experimental study to elicit the infrared properties of H_2O, CO_2 or NH_3 molecules that have been in a single high-energy collision with N_2 or O. The research program was undertaken by Calspan Corporation, Buffalo, New York, under Contract No. F04611-72-C-0035 for the Air Force Rocket Propulsion Laboratory, Director of Science and Technology, Air Force Systems Command, Edwards Air Force Base, California 93523. This program was sponsored by the Advanced Research Projects Agency; Col. Paul Baker, Director, ARPA Plume Physics Program, and monitored by the Air Force Rocket Propulsion Laboratory; Capt. J. R. Nunn and Dr. Lawrence Quinn, technical monitors.

The overall program was divided into three main tasks. The purpose of Task A was to measure the spectral infrared radiation induced by high-speed collisions between rocket exhaust products and atmospheric species. The purpose of Task B was to relate the pure-rotational spectra obtained in Task A to the total plume radiant intensity, determine collisional cross sections for rotational excitation, and extrapolate the results to higher velocities. The purpose of Task C was to measure SWIR spectral radiances and other supporting diagnostic characteristics of rocket plumes in a high-altitude test facility.

A detailed discussion of each task is presented in two separate reports. This report (AFRPL-TR-74-30) describes the results of Tasks A and B. A report (AFRPL-TR-74-31) to be issued later will describe the results of Task C.

The authors wish to acknowledge the assistance of Miss Marcia Williams in the analysis of the rotational spectrum.

TABLE OF CONTENTS

LIST OF ILLUSTRATIONS

LIST OF TABLES

1. INTRODUCTION

The experiment that is described here was designed to elicit the infrared radiative properties of molecules of H_2O, CO_2 or NH_3 that have been involved in a single high-energy collision with N_2, O, or Argon. A pressure-driven reflected-shock tunnel was used to produce N_2 molecules at a velocity of 5.8 Km/sec, O atoms at 4.3 Km/sec, argon at 5.4 Km/sec at sufficiently low density that the effect of single collisions could be observed. A liquid nitrogen cooled flat plate, containing the H_2O, CO_2 or NH_3 injector and a Ge:Hg infrared detector, was aligned with the flow in the test section. A second flat plate, also cooled with liquid nitrogen, was placed parallel to the first plate and served as a cooled background for the detector.

For the experimental arrangement just described, the energy transferred to rotational excitation of the target molecule is close to the maximum for this type of collision. Viewed in the center-of-mass coordinate system, such a collision results in both particles emerging from the interaction zone with little residual velocity. In the laboratory system both particles, and in particular the excited target molecule, move with a velocity close to that of the center of mass. Since the initial velocity of the target molecule is an order of magnitude smaller than the approaching N_2 molecule, O atom or Argon, the center-of-mass velocity is approximately aligned with the velocity of the N_2, O or Argon stream. Thus the excited target molecules travel downstream nearly parallel to the direction of the bombarding stream.

One can take advantage of this special feature of these collisions to design an experiment in which excited states are generated at one streamwise location and the associated radiation intensity viewed by an infrared detector at a location farther downstream. The design limitations, then, are related to the lifetime of the excited state as compared with the transit time to (and through) the field of view of the detector, and to the probability of collisional deexcitation.

In Section 2, the experimental apparatus and diagnostic techniques used to obtain these results are described. Section 3 discusses the data reduction procedure used to convert the detector output to the appropriate

values of the ratio of cross section for collisional excitation to the lifetime of the participating excited state (σ_* / τ) and Section 4 discusses the theoretical calculations utilized to go from values of (σ_* / τ) to values for the excitation cross section σ_* . Section 5 presents the experimental data for the interaction of N_2 -H_2O, N_2 -CO_2, N_2-NH_3, O-H_2O, and Ar-H_2O. The Appendix provides some semi-empirical formulae which permit correlation of vibrational relaxation data and collisional excitation cross sections.

2. EXPERIMENTAL APPARATUS AND TECHNIQUE

2.1 Shock-Tunnel Measurements

The shock-tunnel used in this work utilizes a 3-inch internal diameter by 42 feet long pressure-driven shock tube as its gas supply. For these nitrogen experiments the driver gas was hydrogen at 10,000 psi and 670°K, and the driven gas initial pressure was 30 torr and room temperature. For the oxygen experiments the driver gas was helium at 12,000 psi and 670°K, and the driven gas initial pressure was 30 torr and room temperature. For the argon experiments the driver gas was hydrogen at 12,000 psi and 670°K, and the driven gas initial pressure was 30 torr and room temperature.

Flow is initiated by rupturing the double diaphragms which initially separate the driver and driven gases. The tunnel is of a two-stage design. The initial two-dimensional expansion allows the flow to expand to a nominal Mach number of 3.5. This flow is then turned through 10° by a Prandtl-Meyer expansion on a flat plate, the center portion of this flow being collected by the entrance stage of a conical nozzle. The final diameter of the nozzle is six feet and a twenty feet long constant diameter dump tank is attached to the nozzle at this diameter. The flat-plate model used in this work is shown in Figure 1 and was located just downstream of the nozzle exit plane.

Because of the high-enthalpy conditions of interest in this study, it was known that the available test time would be relatively small. It was felt to be essential to the success of the study that the d· · ion and uniformity of the test-gas flow be determined experimentally. efore, several diagnostic experiments were performed for the shock-tube flow and for the nozzle flow in order to define the parameters of interest.

Shock-tube measurements were performed in order to establish the shock-wave diagram (distance-time) for the high-enthalpy conditions. An unfiltered 1P28 photomultiplier tube was used to monitor the incident-shock radiation intensity. Six photodiodes were used to monitor the reflected-shock radiation intensity in the wavelength range 0.36 to 1.1 microns. One of the diodes was located in the end wall so as to view the radiation intensity parallel

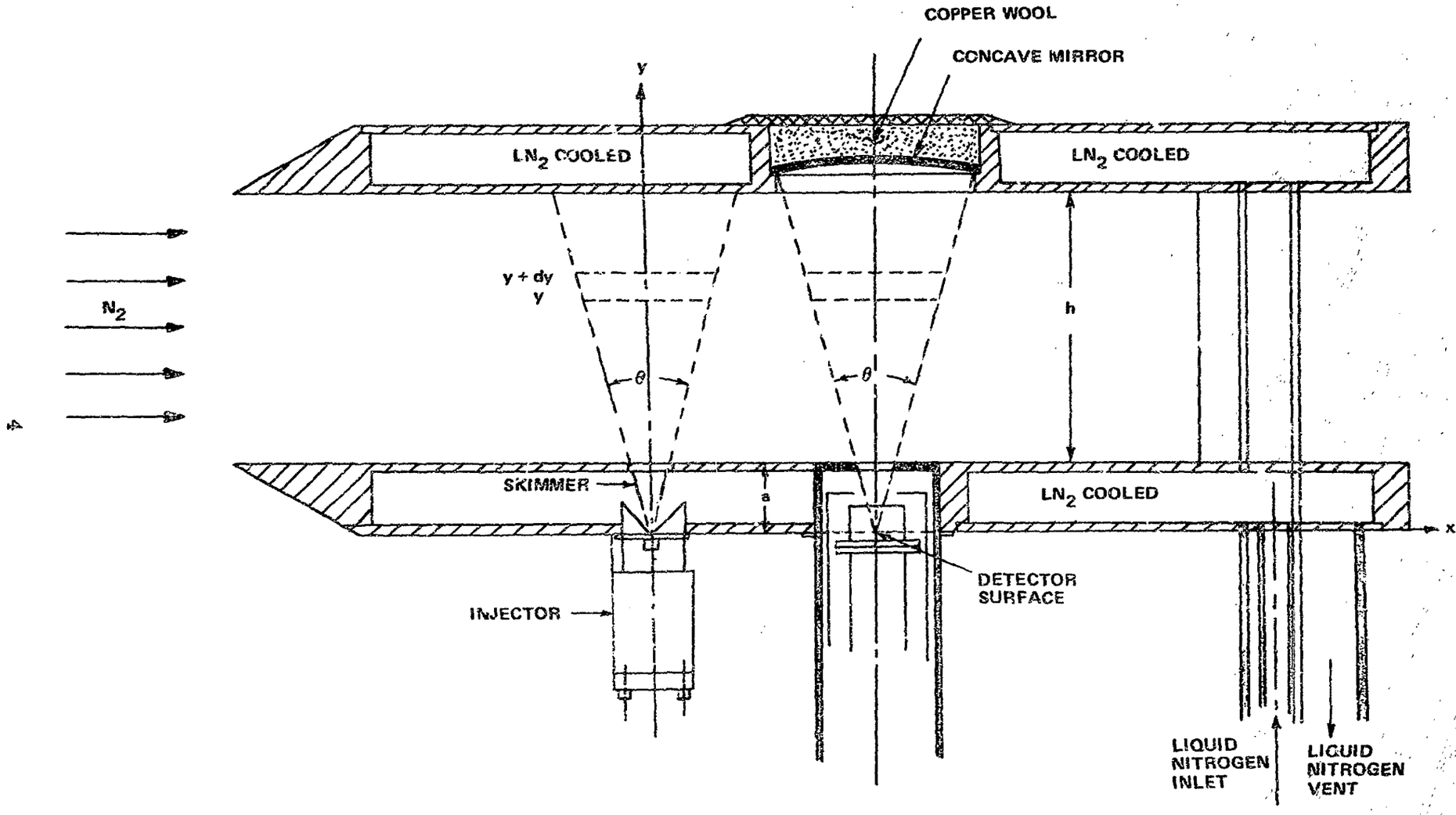

Figure 1 SCHEMATIC OF THE EXPERIMENT

to the shock-tube axis. The remaining photodiodes were located in the side wall so as to view the reflected-shock processed gas normal to the tube axis at 0.62, 1.12, 1.62, 3.88 and 4.88 inches from the end wall. A flush-mounted pressure transducer was located in the end wall in order to measure the reflected-shock pressure history. The data obtained from these detectors made it possible to construct the appropriate shock-wave diagrams and ascertain the uniformity and duration of the reflected-shock test slug.

Figures 2 and 3 illustrate the characteristics of the oscilloscope records obtained using nitrogen as the test gas at a reflected-shock reservoir condition of 8600°K at 85 atm pressure. The corresponding value of the maximum velocity to which the test gas could be expanded ($\sqrt{2H_{reservoir}}$) was about 6.5×10^5 cm/sec. However, at this test condition, the velocity realized in the test section was calculated to be 5.8×10^5 cm/sec (this value has been confirmed experimentally as will be described later in this section), reduced from 6.5×10^5 cm/sec, because of the energy frozen in dissociation of 13 per cent of the nitrogen molecules at the test location. Figure 2(a) illustrates the uniformity and duration of the incident-shock radiation intensity measured upstream of the end wall, Figure 2(b), is the reflected-shock pressure measured at the end wall, and Figure 2(c) is the radiation intensity measured after shock reflection looking from the end wall. Figure 3(a) through (d) are the radiation-intensity histories measured after shock reflection looking normal to the tube axis at 0.62, 1.12, 1.62 and 4.9 inches from the end wall. The data presented in Figures 2 and 3 are used to construct the wave diagram shown in Figure 4. The reflected-shock test time can be seen to be on the order of 100 μsec for this condition.

Experiments were also performed at shock-tube conditions that resulted in somewhat lower test-section particle velocities but increased test time. This test condition will be used to study the influence of N_2 velocity on the infrared radiation observed from the excited target molecules. The shock-wave diagram obtained for this condition, which resulted in a test-section velocity calculated to be 5.2×10^5 cm/sec, is shown in

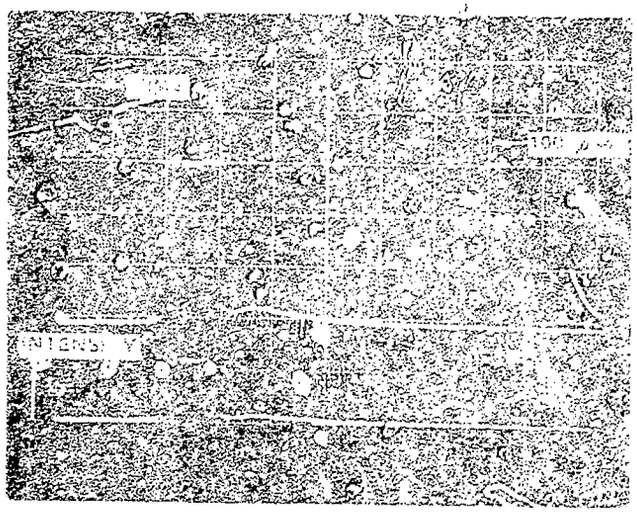

(a) INCIDENT-SHOCK RADIATION INTENSITY AT 15.5" FROM END WALL

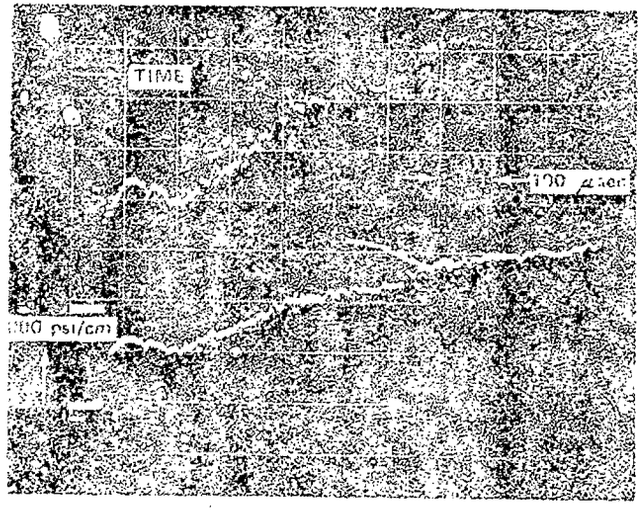

(b) REFLECTED-SHOCK PRESSURE AT END WALL

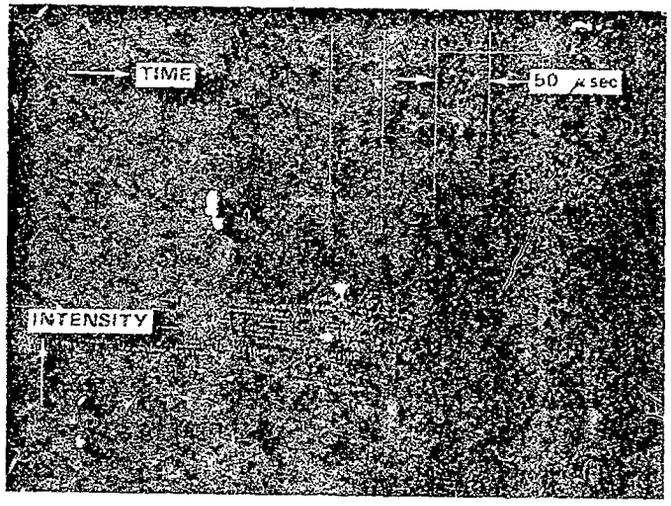

(c) RADIATION INTENSITY AFTER SHOCK REFLECTION LOOKING FROM END WALL

Figure 2 MEASUREMENTS IN NITROGEN TEST GAS FOR T_{REF} = 8600 ^{o}K AT 85 ATM

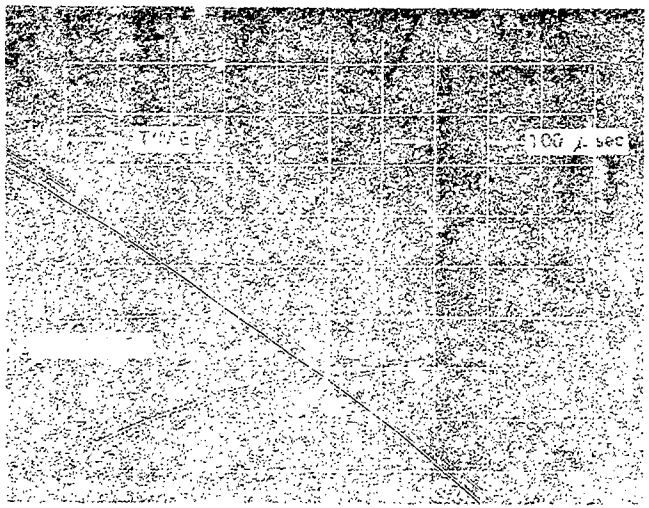

(a) RADIATION INTENSITY AT 0.62" FROM END WALL

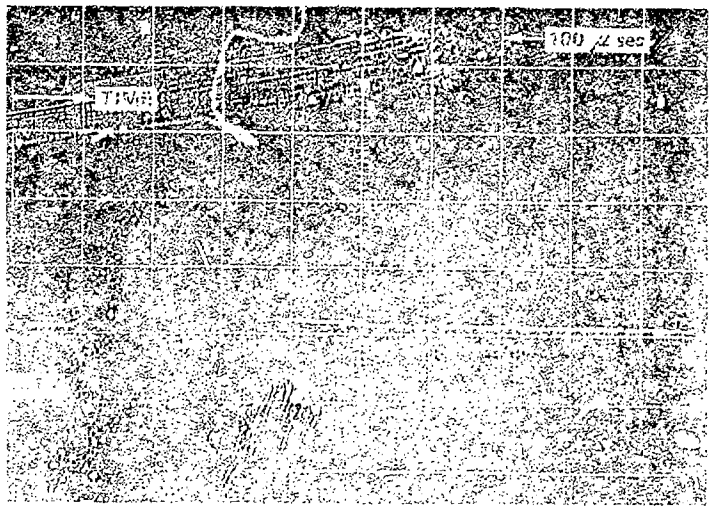

(b) RADIATION INTENSITY AT 1.12" FROM END WALL

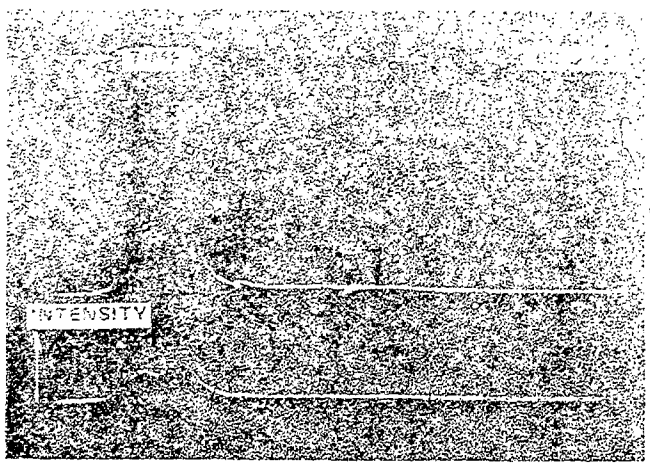

(c) RADIATION INTENSITY AT 1.62" FROM END WALL

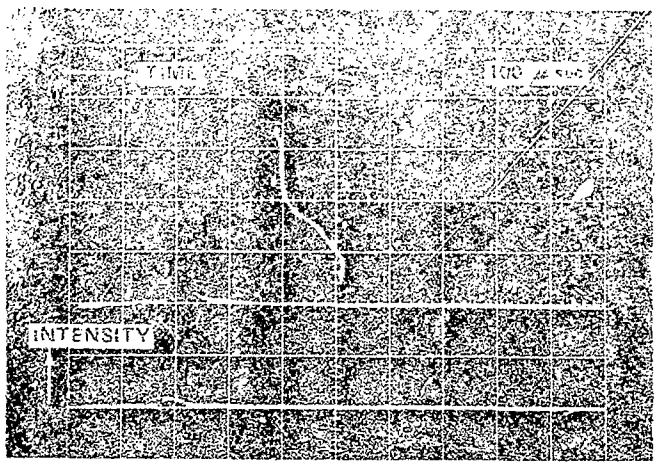

(d) RADIATION INTENSITY AT 4.9" FROM END WALL

Figure 3 REFLECTED-SHOCK MEASUREMENTS IN NITROGEN

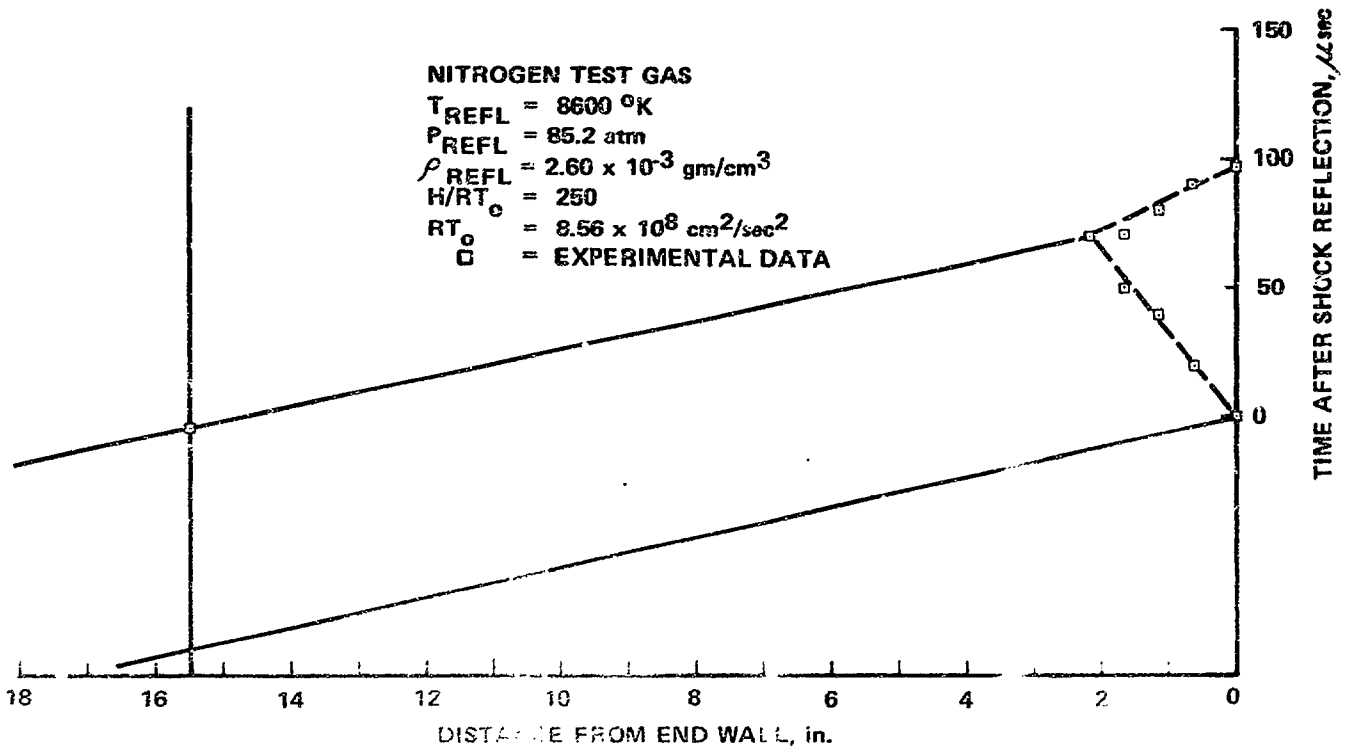

Figure 4 SHOCK-WAVE DIAGRAM OBTAINED FROM EXPERIMENTS

Figure 5. It is of interest to compare these results with those of Figure 4 and note the reduction in reflected-shock test time with increasing reservoir-enthalpy level.

The transient starting process[1,2] of the nozzle is an important consideration because of the potential influence on the available test time. Therefore, measurements necessary for the determination of the starting process were obtained using nitrogen as the test gas. As part of this work, the test-gas particle velocity as well as the duration and uniformity of the flow were obtained in the test section at the flat-plate location. The diagnostic tools used in this work were thin-wire Langmuir probes and piezoelectric pressure transducers. The wire probes were 0.004 in. diameter by 0.400 in. in length and were aligned with the flow direction. Two of these probes were biased at +1 volt so as to collect electrons. By placing the probes a known axial distance apart and by assuming the plasma to be neutral, the particle velocity could be determined by observing the small fluctuations in test-flow electron density. The nonuniformities in the electron-density history, observed at both axial stations, can be readily used to estimate the particle velocity. These data were recorded on oscilloscopes at sweep rates such that the velocity could be determined within the necessary accuracy.

A third electrostatic probe was placed in the test flow and the voltage applied to this probe was swept from -5 to +2 volts during the test flow so that the electron density and electron temperature could be determined. Figures 6 and 7 illustrate the oscilloscope records from which the electron-density and electron-temperature results were deduced using the free-molecular flow theory of Laframboise.[3] The probe output was recorded on two oscilloscopes so that the ion-current region could be separated, and recorded on a more sensitive scale, from the electron-retarding and electron-current regions of the probe characteristic. The electron temperature was found to be approximately 1300°K reflecting a nitrogen vibrational temperature of the same order as compared with a calculated heavy-particle temperature of approximately 230°K. The

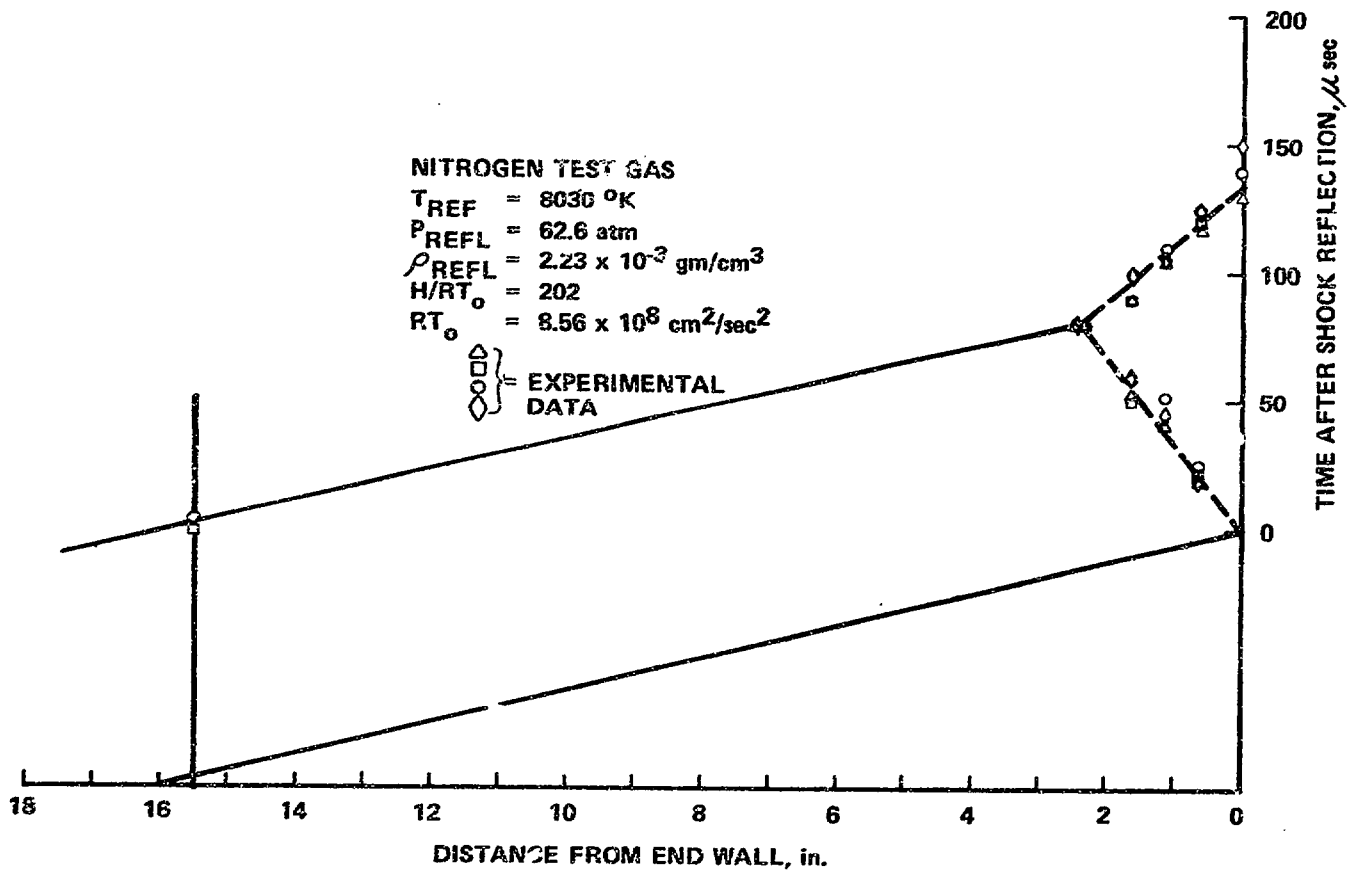

Figure 5 SHOCK-WAVE DIAGRAM OBTAINED FROM EXPERIMENTS

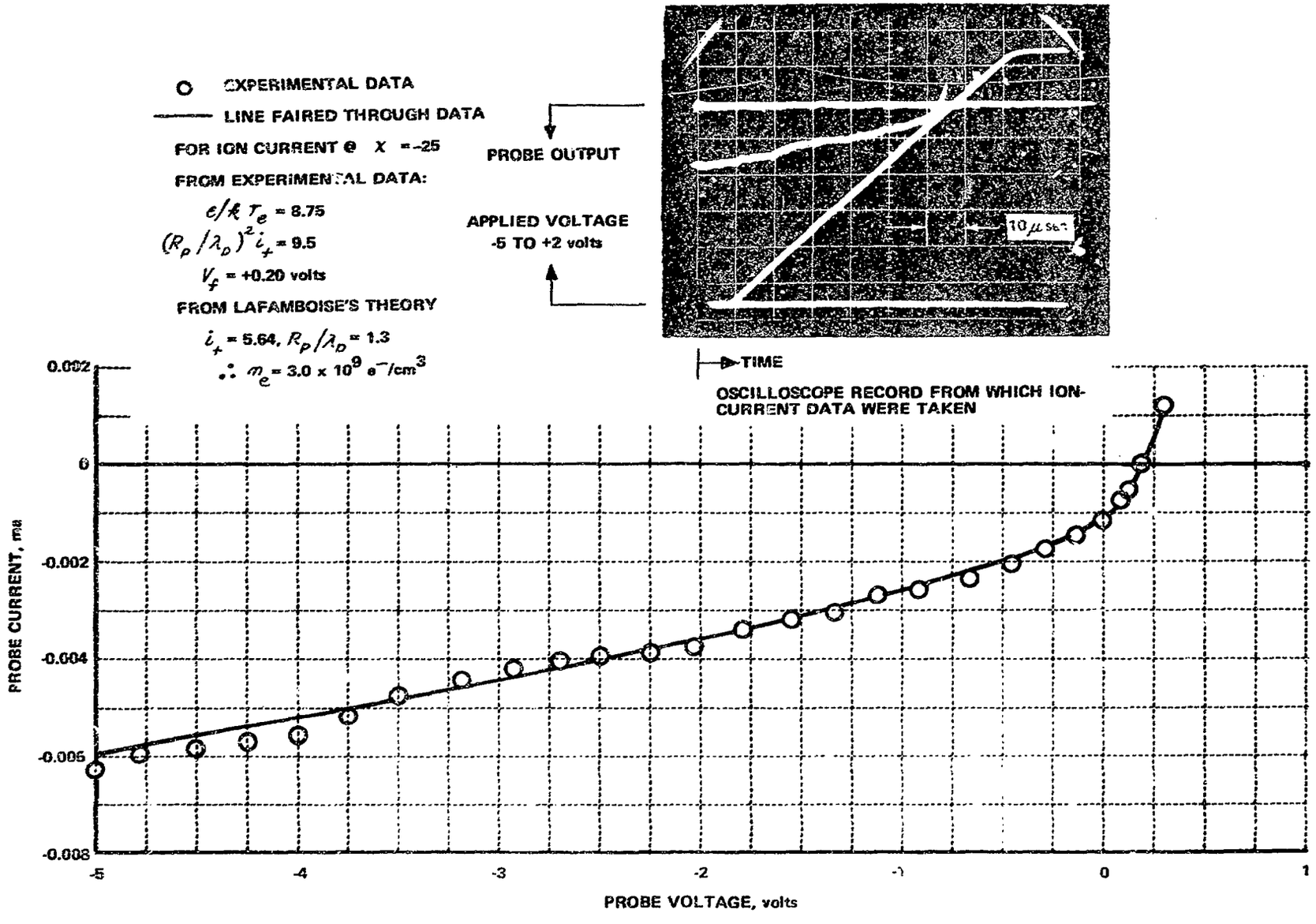

Figure 6 ION-CURRENT REGION OF EXPERIMENTAL PROBE CHARACTERISTIC

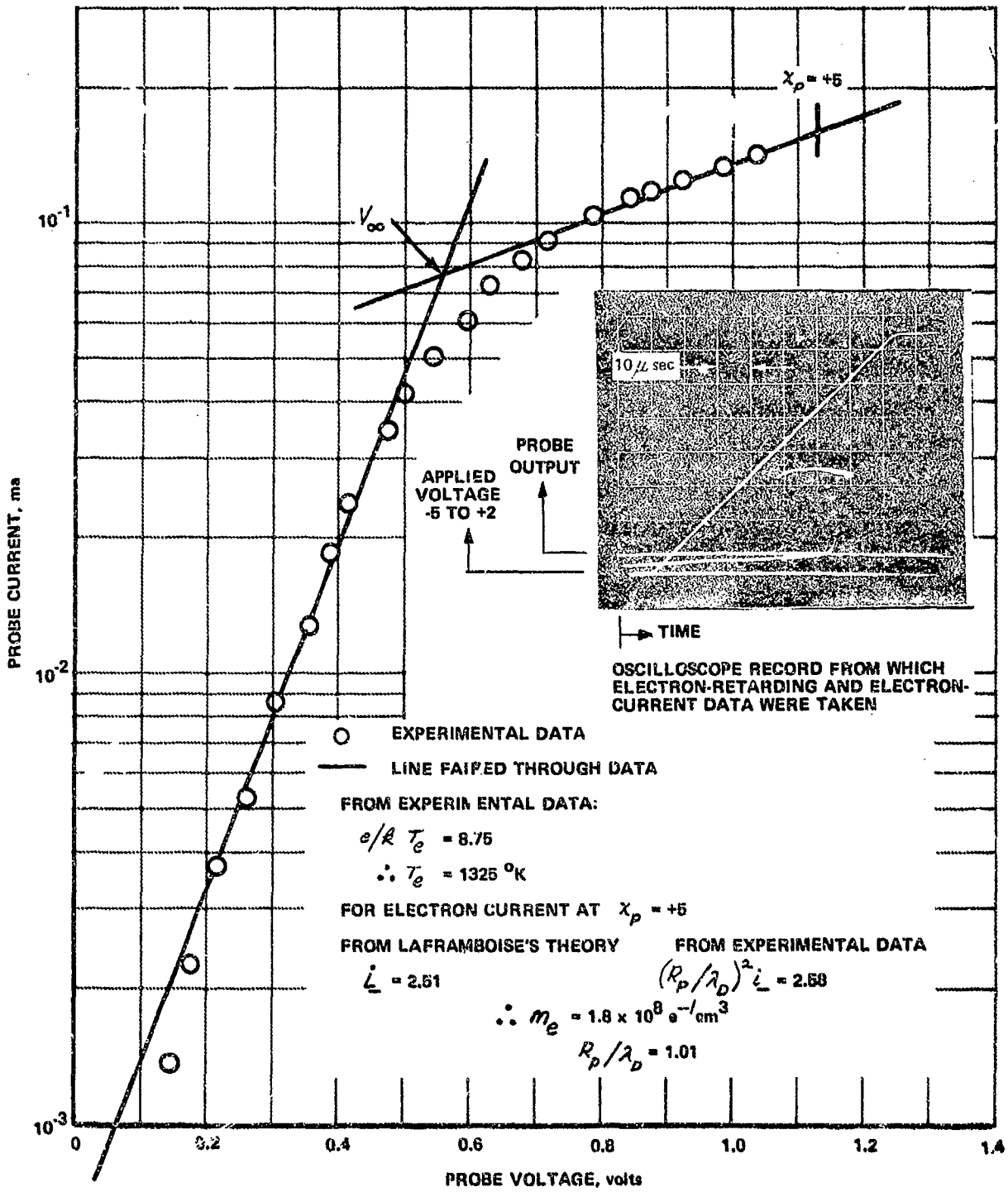

Figure 7 ELECTRON-RETARDING AND ELECTRON-CURRENT REGIONS OF EXPERIMENTAL PROBE CHARACTERISTIC

electron density deduced from the ion-current region of the probe characteristic was 3×10^9 e^-/cm^3 compared with 1.8×10^9 e^-/cm^3 obtained from the electron-current region. This agreement between the electron-density values obtained from these two portions of the probe characteristic is satisfactory for the purpose of ascertaining the appropriate expansion parameters. Additional experiments were conducted for which better agreement was achieved between the electron density determined from these two portions of the current-voltage characteristic.

In addition to the Langmuir-probe measurements, the pitot pressure was measured using flush-diaphragm piezoelectric transducers in order to provide for a check on the gas density, since the pitot pressure is proportional to ρu^2 , and the spanwise flow uniformity. Since the particle velocity was known from the Langmuir-probe measurements and confirmed by nonequilibrium-flow calculations and since the specific heat ratio could be calculated, the gas density was easily determined within the necessary accuracy. The gas density determined in this manner was then compared with the results of an inviscid-flow calculation in order to determine the appropriate expansion area ratio for our experimental conditions. To provide a check on this determination, the calculated electron density at the area ratio determined from the pitot-pressure measurements was compared with the measured electron density and found to be in good agreement.

Both the electrostatic-probe and the pitot-pressure measurements indicated that approximately ten to fifteen percent of the available test time was consumed in the starting process. It was thus concluded that the transient starting process of the nozzle would not adversely influence the available test time at these high-enthalpy conditions. Further, the electron density as a function of time was found to have only minor fluctuations in the test flow suggesting good test-flow uniformity.

2.2 Detector and Filter Calibration

The infrared detector used in these experiments was a liquid helium cooled mercury doped germanium detector. As illustrated in Figure 8, the

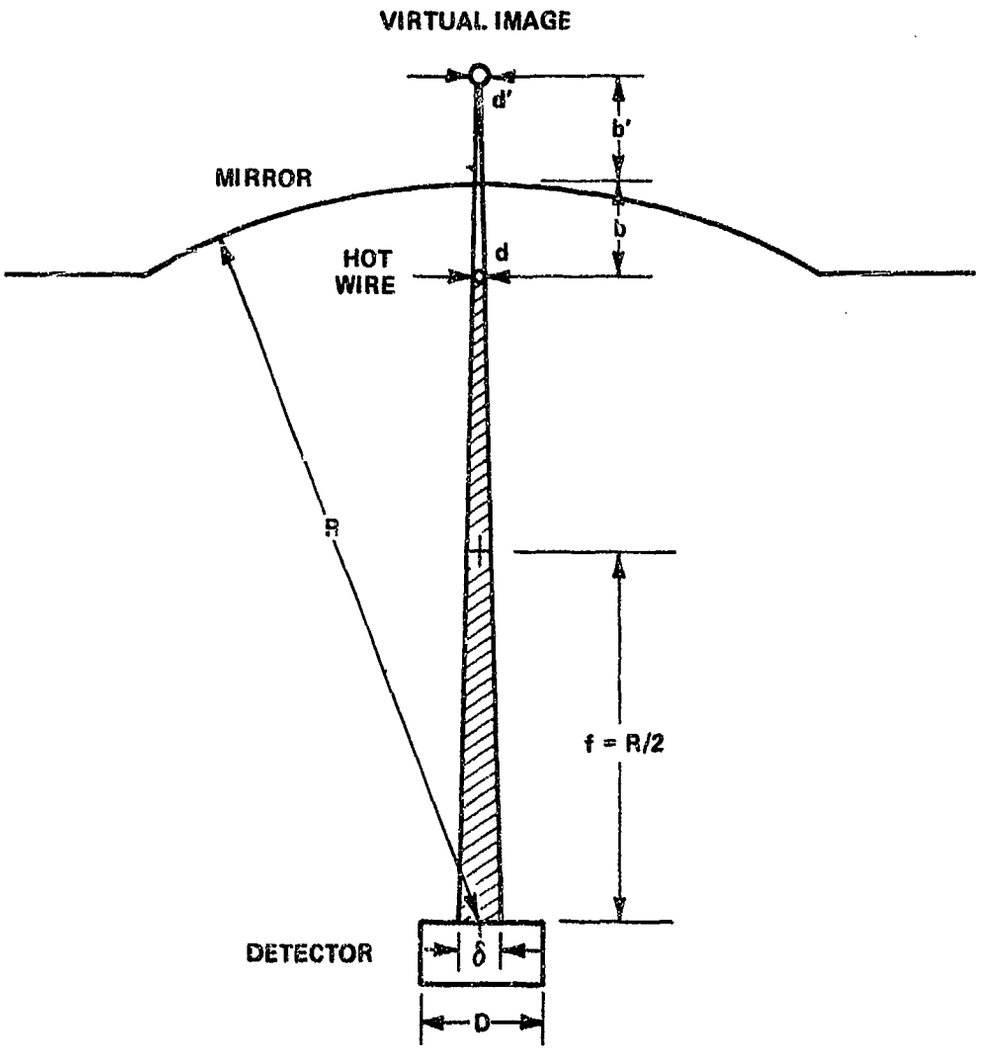

Figure 8 SCHEMATIC OF DETECTOR CALIBRATION (NOT TO SCALE)

field of view of the detector was terminated at the opposite wall of the model by a surface-silvered spherical mirror whose center of curvature was approximately coincident with the detector chip. The purpose of this mirror was to minimize diffused reflection of radiation into the detector, which could have occurred since the LN_2-cooled model was suspended in a vacuum tank at room temperature. Provided the surface of the mirror did not frost, the only background radiation that could enter the detector, in principle, had to come from the surface of the mirror. The mirror was backed by a pad of copper mesh to keep it in good thermal contact with the LN_2-cooled model.

For these experiments the radiation intensity was observed in the region from 2.5 to 14.0 μ using eight different filters. The half-power points for each of these filters are: (1) 2.5 to 3.1 μm, (2) 4.28 - 4.34 μm, (3) 5.7 to 7.5 μm, (4) 8.3 to 9.2 μm, (5) 8.3 to 14.0 μm, (6) 9.1 to 10.3 μm, (7) 10.6 to 11.6 μm and (8) 11.1 to 14.0 μm. The field of view of the detector is 30° and a 2 mm thick Irtran 2 window, cooled to liquid nitrogen temperature, separates the detector shroud from the test flow. For each experiment, one of the eight previously mentioned filters, cooled to near liquid helium temperature, is placed between the detector and the Irtran 2 window in the field of view. It was therefore necessary to perform calibration experiments for each of the filters by employing a known input radiant flux of the same order as expected in the experiment. This input signal was provided by a platinum wire, 0.0001 inch in diameter by 0.100 inch in length, placed in the FOV and electrically heated to provide the necessary radiant flux. By measuring the wire resistance and knowing the spectral emissivity[4] of platinum as a function of temperature, it was possible to calculate the radiant flux emitted by the wire over each bandwidth using the equations presented above.

In order to compute the appropriate area of the radiating surface it was important to review the calibrating system in detail. If the system were perfectly aligned the hot wire would cast its shadow across the center of the detector, in the radiation reflected from the mirror. If imperfectly aligned, that shadow could miss the detector completely and there would be no loss. The maximum possible loss caused by the shadow is very small, since the wire diameter, d , was 0.0001 inch. Considering the

radiation from a point on the surface of the virtual image, noting that the wire length, L, is an order smaller than the other dimensions, the width, δ, of the shadow is given by

$$\frac{\delta}{d} = \frac{R + b'}{b + b'} \tag{1}$$

Now, since $R = 2f$, where f is the focal length, and $\frac{1}{f} = \frac{1}{b} - \frac{1}{b'}$, Eq. (1) can be written

$$\frac{\delta}{d} = \frac{\frac{R}{b} - 1}{2\left(1 - \frac{b}{R}\right)} \tag{2}$$

The approximate values were

$$R = 5\text{-}1/2 \text{ inches}$$
$$b = 1/2 \text{ inch}$$

making

$$\frac{\delta}{d} = 5\,\tfrac{1}{2} \tag{3}$$

The detector aperture is square with

$$D = 0.25 \text{ cm}$$

The wire diameter is

$$d = 0.0001 \text{ inch}$$

Thus the maximum fractional loss of radiation from the image was

$$\frac{\delta D}{D^2} = \frac{\delta}{d}\,\frac{d}{D} = \frac{11}{2} \times \frac{10^{-4} \times 2.54}{0.25} = 5.6 \times 10^{-3} \tag{4}$$

Since the radiation from the wire and its image are roughly equal at the detector, the correction for the shadow effect is about (1/4)% and was, therefore, neglected.

The power radiated into the detector from the hot wire and its image is readily obtained in terms of the radiance of the surface, N_λ . Assuming the wire to be a Lambertian surface (which is probably not quite accurate beyond 50° from the normal) the power radiated into the detector in the wavelength interval $\Delta\lambda$ is given by

$$P_\lambda \Delta\lambda = L d N_\lambda \Delta\lambda A_d \left[(R - f)^{-2} + (R + f')^{-2} \right]$$

$$\therefore P_\lambda \Delta\lambda = \frac{2 L d N_\lambda \Delta\lambda A_d}{R^2} \qquad (5)$$

where terms of order $\frac{f^2}{R^2}$ have been neglected.

Now

$$N_\lambda \Delta\lambda = \frac{1}{\pi} \epsilon_\lambda I_\lambda \Delta\lambda$$

where ϵ_λ is the spectral emissivity of platinum[4] at wavelength λ , and I_λ is the blackbody spectral radiant emittance given[5] by

$$I_\lambda = \frac{C_1}{\lambda^5} \frac{1}{e^{C_2/\lambda T} - 1} \qquad (6)$$

where T is the wire temperature (°K) and

$$C_1 = 3.74 \times 10^4 \text{ watts } \mu^4 \text{ cm}^{-2}$$

$$C_2 = 1.438 \times 10^4 \ \mu \text{ °K}$$

Combining Eqs. (5) and (6),

$$P_\lambda \Delta\lambda = \frac{2 L d A_d}{\pi R^2} \epsilon_\lambda \frac{C_1}{\lambda^5} \frac{\Delta\lambda}{e^{C_2/\lambda T} - 1} \qquad (7)$$

Figures 9-11 illustrate the detector output in millivolts measured as a function of average photon flux for the 2.5 to 3.1 μ, 8.3 to 9.2 μm,

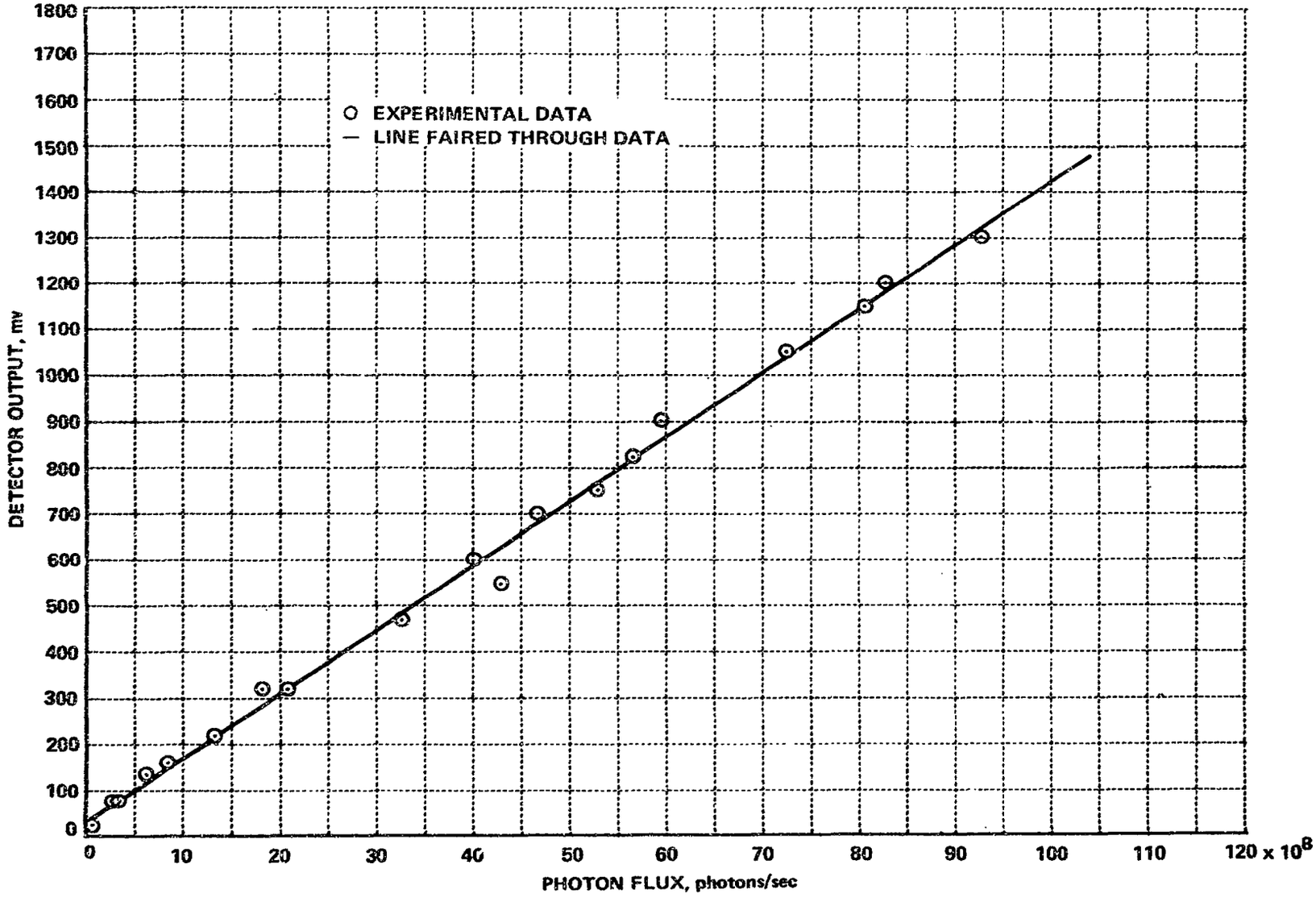

Figure 9 CALIBRATION RESULTS FOR Ge:Hg DETECTOR AND 2.5 TO 3.1 μ FILTER

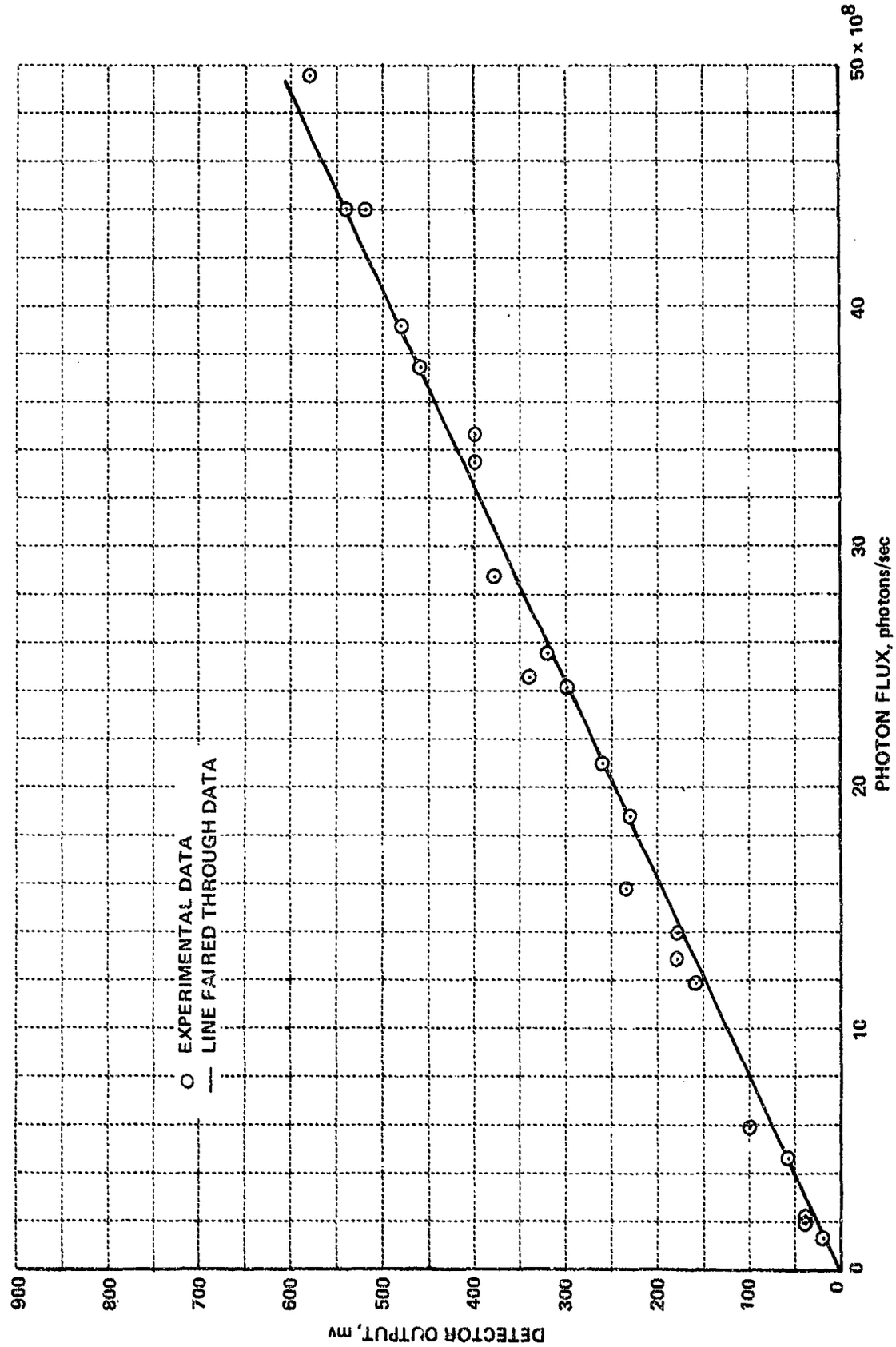

Figure 10 CALIBRATION RESULTS FOR Ge:Hg DETECTOR AND 8.3 TO 9.2 μ FILTER

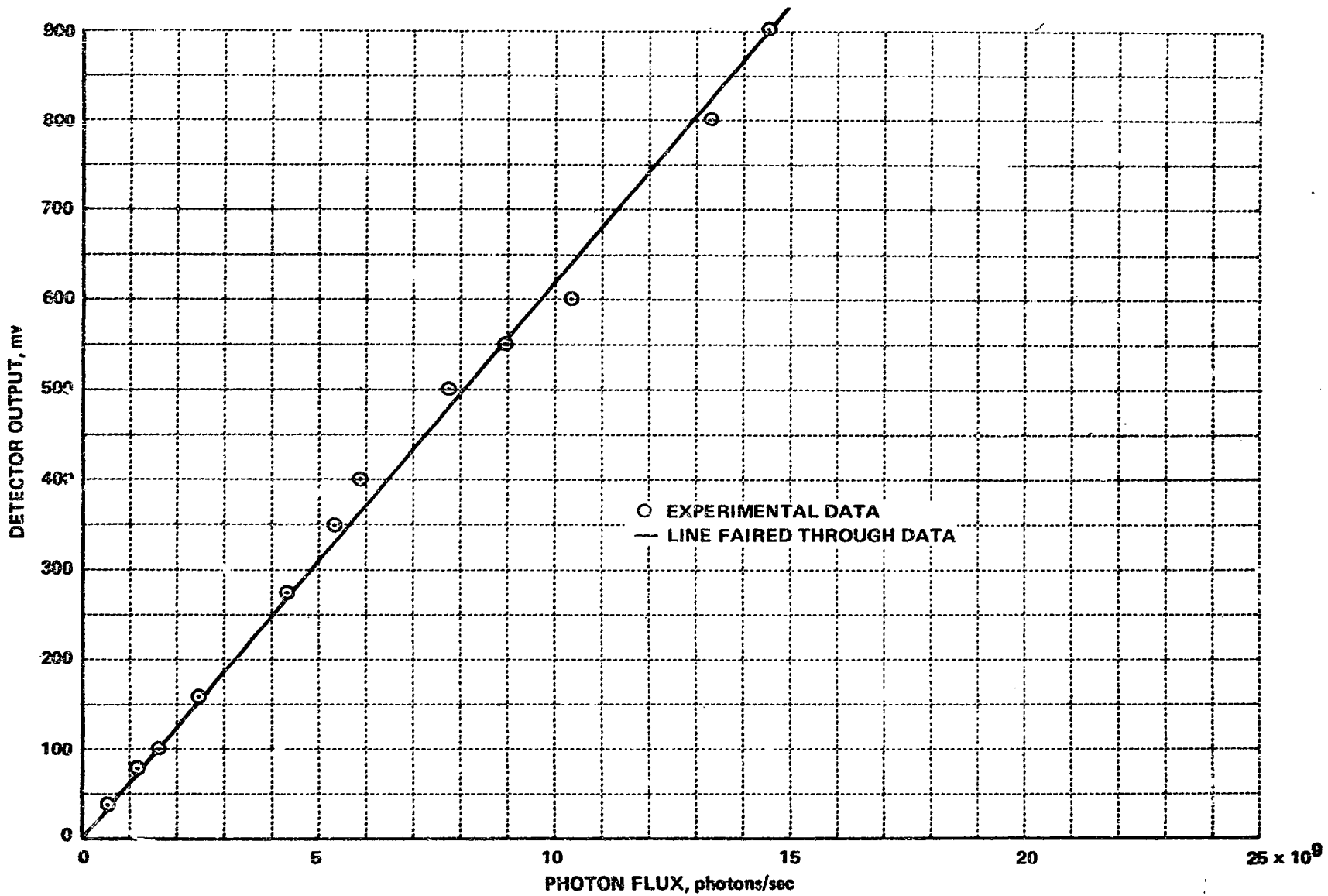

Figure 11 CALIBRATION RESULTS FOR Ge:Hg DETECTOR AND 8.3 TO 14.0 μ FILTER

and 8.3 to 14 μm filters. The calibration results are representative of the remaining filters and all were found to be linear with relatively small deviations occurring at the low signal levels.

Figure 12 is typical of the calibration data obtained as part of this study. These particular results are for the 8.3 to 9.2 μm filter. Figure 12(a) is the detector output signal obtained with the platinum wire at 77°K and the remaining background also at 77°K. Figure 12(b) is the signal received for a wire temperature of 590°K (photon flux of 2.1×10^9 photons/sec) and Figure 12(c) is a corresponding oscilloscope data record for a wire temperature of 736°K (photon flux of 2.9×10^9 photons/sec). The radiant flux recorded is shown to remain nearly constant for at least 15 millisec. indicating that conduction cooling does not significantly influence the calibration results. For a given wire resistance (or temperature) the calibration results were independent of whether the wire was being heated or cooled.

2.3 Measurement of Injected-Gas Flow Rates

The number of target molecules, n_2, entering the path of the incident stream and the velocity, v_2, of these target molecules must be known in order to deduce values of σ_* / τ from the experimental results. Section 3 provides a complete description of the data reduction procedure and the importance of these parameters can be found in that section. The purpose of this discussion is to describe the experimental techniques used to obtain the values appropriate to these experiments.

In order to determine the H_2O, CO_2 or NH_3 particle density and time history, an ionizer built in the form of a cube was placed flush with the plate surface at the outlet of the injector. The opening into the ionizer was just slightly larger in diameter than the injector outlet. A beam of 80 e.v. electrons was established in the ionizer and the injector was operated. This permitted the target gas to flow and the collected ion and electron currents were monitored on an oscilloscope. Figure 13 is typical of the results obtained for H_2O, CO_2, and NH_3 injection. The time at which the N_2 arrives at the injector location for the 5.8 Km/sec

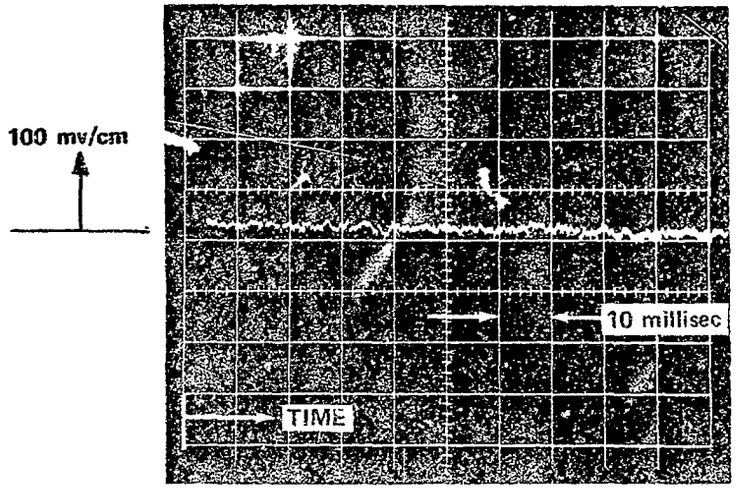

(a) DETECTOR SIGNAL FOR 77 ^{o}K BACKGROUND

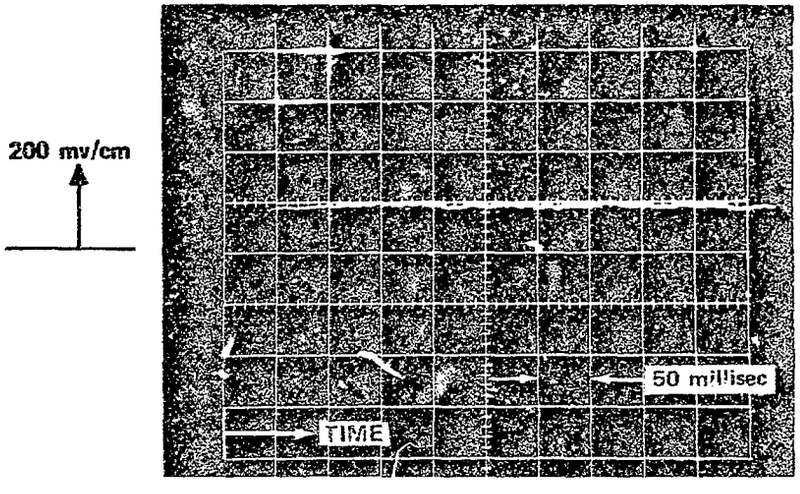

(b) PHOTON FLUX = 2.1 x 10^{9} *photons/sec*

WIRE RESISTANCE = 102.4 Ω
WIRE TEMPERATURE = 590 ^{o}K
WIRE EMISSIVITY = 0.054

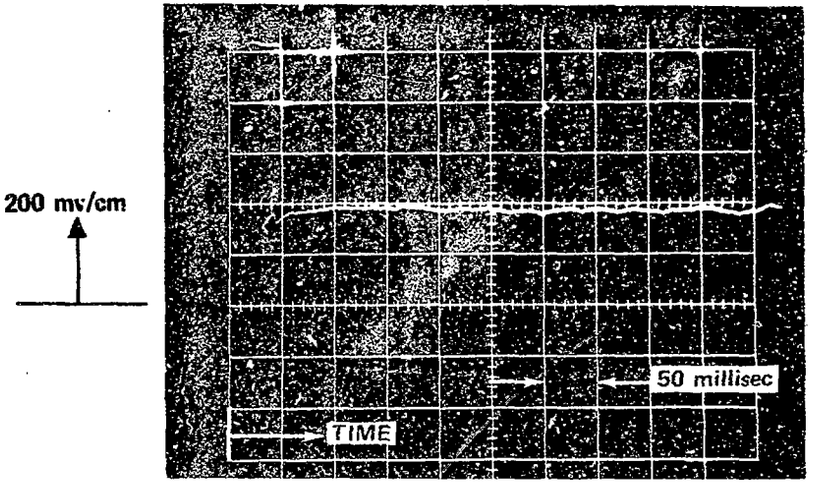

(c) PHOTON FLUX = 2.9 x 10^{9} photon/sec

WIRE RESISTANCE = 127.2 Ω
WIRE TEMPERATURE = 736 ^{o}K
WIRE EMISSIVITY = 0.063

Figure 12 TYPICAL DETECTOR CALIBRATION DATA FOR 8.3 TO 9.2 μ FILTER

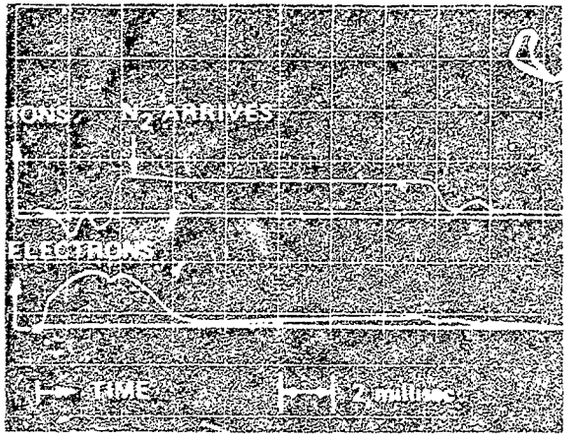

a) H_2O FLOW HISTORY

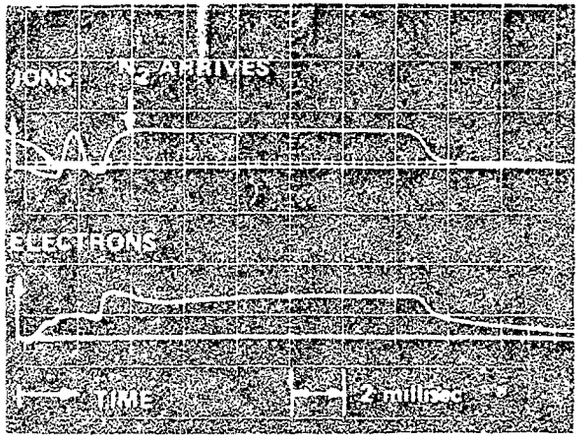

b) CO_2 FLOW HISTORY

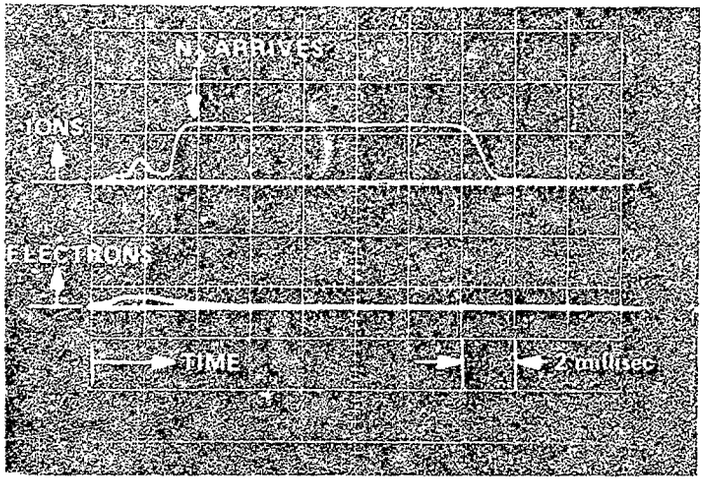

c) NH_3 FLOW HISTORY

Figure 13 CALIBRATION DATA FOR H_2O, CO_2, AND NH_3 BEAMS

experiments is shown on these data records. For the lower velocity experiments the arrival of incident stream particles will occur at a later time. In order to convert the measured ion current to particle density, the ionizer was filled with a known density of air molecules and the current measured. Knowing the ionization cross sections[6,7] as a function of electron energy for all of the species involved, the H_2O, CO_2 and NH_3 particle densities were determined at the location $(a+\ell)$ where (a) is the distance between the x-axis and the plate surface and (ℓ) is the ionizer length. The inverse square law can then be used to determine the particle density at the plate surface using a straightforward calculation.

The velocity of the target molecules, v_2, was calculated from the expression $v_2 = \sqrt{\frac{2}{\gamma-1}}\, a_o$ where a_o is the speed of sound in the injector reservoir. In order to ascertain a_o it was necessary to measure the temperature of the gas in the injector when the plates were cooled to liquid nitrogen temperature. To make this measurement, a platinum wire 0.0001 inch in diameter by 0.10 inch in length was supported between two needles and placed in the injector chamber. The temperature coefficient of resistivity of platinum is well known but was independently checked (from room temperature to 77°K). By measuring the wire resistance at room temperature and after the plates had reached a steady-state temperature, it was possible to infer the injector gas temperature and thus a_o. The temperature of H_2O vapor was found to be 343°K (higher than either the CO_2 or NH_3 vapor temperature because hot water was circulated through the injector jacket for the H_2O experiments but not for the CO_2 or NH_3 experiments), the temperature of the CO_2 vapor was found to be 217°K and for the NH_3 vapor the measured temperature was 215°K. The appropriate values of the specific heat ratio were taken from Ref. 8 for H_2O and CO_2 and from Ref. 9 for NH_3.

3. ELEMENTARY THEORY OF THE INFRARED MEASUREMENTS

The theory of the infrared measurements reported here is based on the approximation that the excited target molecules, whose radiation was observed, traveled from their point of excitation parallel to the x-axis at the center-of-mass velocity, v_* . It is assumed that the lifetime, τ , of any participating state is long compared with the transit time to, and through, the field of view. A cross section, σ_* , is assigned to each excitation of interest.

The schematic of the experiment is shown in Figure 1. The x-axis lies a distance (a) below the surface of the lower plate, and passes through the effective origin of the target-gas stream and through the apex of the field of view, both of which are conical with the same apex angle, θ .

The target stream is attenuated by collisions with the high-speed N_2, O or Ar stream, and essentially vanishes before reaching the upper plate. These collisions are primarily elastic, involving the normal gas-dynamic cross section, σ_o . It is tacitly assumed that the cross sections for exciting the states of interest in these experiments, σ_* , are at least an order of magnitude smaller than the gas-dynamic cross section. Thus the production of excited states does not affect the distribution of target molecules.

The number of target molecules entering the slice of the cone between y and $y + dy$ is $\psi_2(y)$ per second. The probability that a target molecule will suffer an elastic collision in crossing dy is obtained by considering the distance it travels through the high-speed N_2 stream, which, taking the relative velocity to be approximately that of the N_2 stream, v_1 , is

$$n_1 \sigma_o \frac{v_1}{v_2} dy$$

where the density of N_2 molecules, n_1 , is taken to be constant. This was approximately true because it was a condition of the experiment that

the target stream should not create a shock in the incident N_2, and consequently the probability of collision for an N_2 molecule was kept low, having a maximum at the lower plate of about 1/4.

The loss of target molecules in dy is thus given by

$$-d\psi_2(y) = n_1 \sigma_0 \frac{v_1}{v_2} \psi_2(y)\, dy$$

and since collisions start at $y = a$, the total target flux is obtained by integrating from $y = a$,

$$\int_a^y \frac{d\psi_2(y)}{\psi_2(y)} = -n_1 \sigma \frac{v_1}{v_2} \int_a^y dy$$

Hence

$$\psi_2(y) = \psi_2(a)\, e^{a/\eta}\, e^{-y/\eta} \tag{8}$$

where

$$\eta = \frac{v_2}{v_1} n_1 \sigma_0 \tag{9}$$

The molecules which undergo elastic collisions, upon striking either plate, will essentially be removed for the duration of the experiment either by freezing or by becoming accommodated to the wall temperature, approximately 77°K. Those which undergo collisions resulting in excitations of interest in these experiments will travel from their point of excitation, parallel to the x-axis, and pass through the field of view of the detector at the same height, y, above the lower plate. The probability of radiating in the field of view is proportional to the time of flight through the core and therefore depends on the coordinate z as shown in Figure 14. Thus it is necessary to calculate the flux of excited states as a function of both y and z.

Writing $\phi_*(y, z)$ for the flux of excited molecules passing through a plane normal to the x-axis between the target-stream cone and

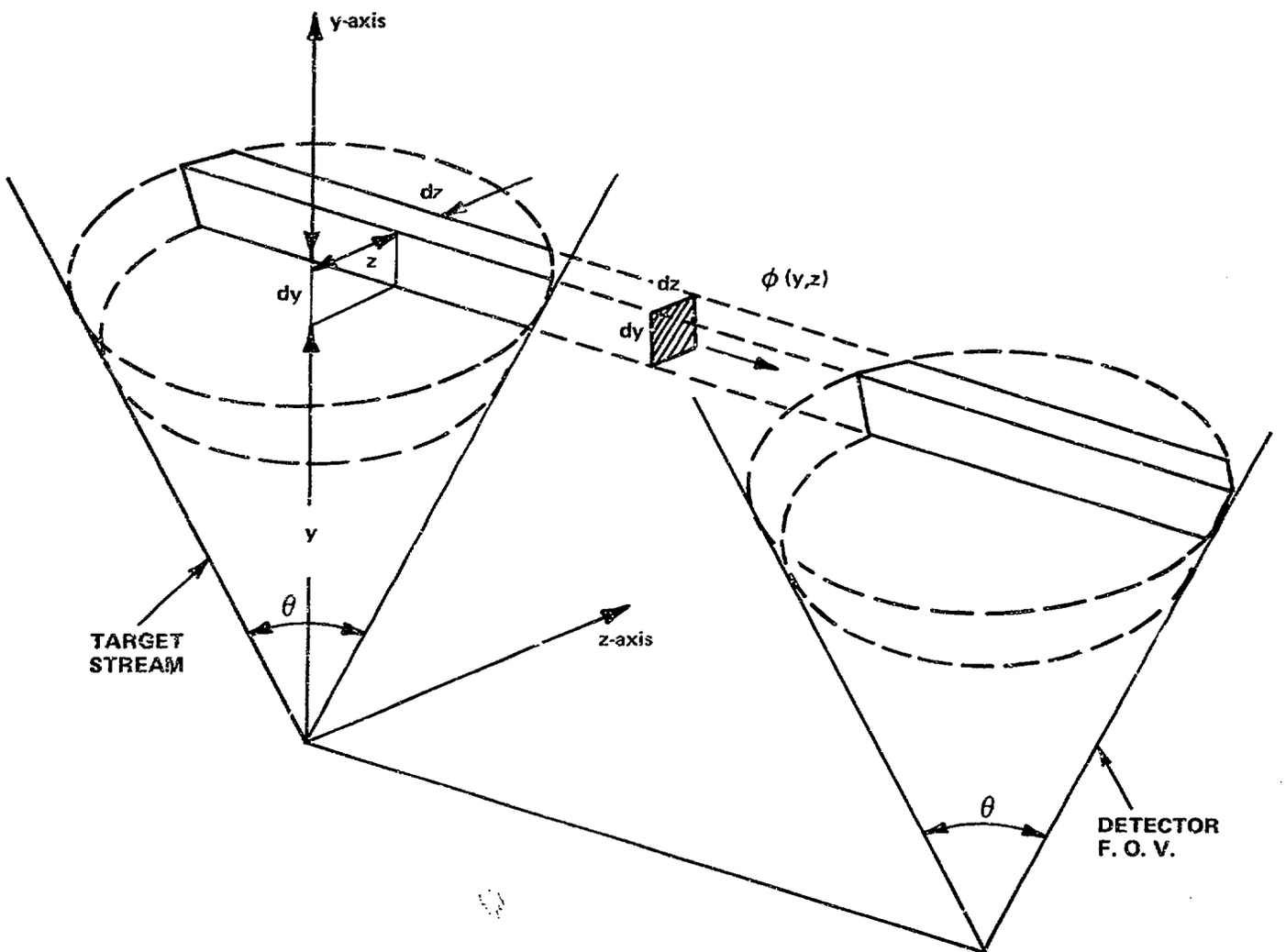

Figure 14 SCHEMATIC FOR CALCULATING THE FLUX OF EXCITED STATES INTO THE FIELD OF VIEW

the field of view, the production of excited molecules can be related to $\phi_*(y, z)$. Since the density, n_1, of N_2 has been assumed constant, the distribution of target molecules is uniform over the section of the first cone at any height y. (Strictly speaking this should be over the spherical cap at constant distance from the apex, but the angle θ will be assumed small enough to justify the above approximation.)

Thus the number of excited molecules produced per second in a small element, $dx\,dy\,dz$, of the target cone is the product of two terms, namely the probability of excitation in traversing dy (which is just the probability of collision with σ_o replaced by the excitation cross section, σ_*) and the flux of target molecules through $dx\,dy$. This product is

$$n_1 \sigma_* \frac{v_1}{v_2} \psi_2(y) \frac{dx\,dy\,dz}{\pi y^2 \tan^2(\theta/2)}$$

The flux emanating from the prism, shown in Figure 14, in the target cone is thus

$$\phi_*(y, z)\,dy\,dz = n_1 \sigma_* \frac{v_1}{v_2} \frac{\psi_2(y)\,dy\,dz}{\pi y^2 \tan^2(\theta/2)} 2\sqrt{y^2 \tan^2(\theta/2) - z^2} \tag{10}$$

Each such excited molecule is exposed to the field of view of the detector for a distance of $\sqrt{y^2 \tan^2(\theta/2) - z^2}$ at the center-of-mass velocity, v_*. Thus the probability of radiating in the field of view is

$$\frac{\sqrt{y^2 \tan^2(\theta/2) - z^2}}{v_* \tau}$$

where the lifetime, τ, is such that this probability is $<< 1$.

Hence the total radiation emanating from the corresponding prism in the field of view is

$$d\omega = \frac{2 n_1 \sigma_* v_1 \psi_2(y)}{\pi v_* \tau v_2 y^2 \tan^2(\theta/2)} \left[y^2 \tan^2(\theta/2) - z^2\right] dy\,dz \tag{11}$$

The fraction of the radiation which actually enters the detector area, A_d , is

$$\frac{A_d}{4\pi y^2}$$

where again the approximation that the distance to the apex is y has been made.

Hence the total photon flux into the detector is given by

$$\omega = \int_a^h \int_0^{y\tan(\theta/2)} \frac{A_d n_1 \sigma_* v_1 \psi_2(y)}{2\pi^2 v_* \tau v_2 y^4 \tan^2(\theta/2)} \left[y^2 \tan^2(\theta/2) - z^2 \right] dz\, dy$$

$$= \frac{A_d n_1 \sigma_* v_1}{\pi^2 v_* \tau v_2 \tan^2(\theta/2)} \int_a^h \psi_2(y) \left[\frac{\tan^3(\theta/2)}{y} - \frac{\tan^3(\theta/2)}{3y} \right] dy$$

$$= \frac{A_d n_1 \sigma_* v_1}{\pi^2 v_* \tau v_2} \frac{4}{3} \tan(\theta/2) \int_a^h \frac{\psi_2(y)}{y}\, dy \qquad (12)$$

It is consistent to make the approximation that $\tan\frac{\theta}{2} \cong \frac{\theta}{2}$, and since $\psi_2(y) \cong 0$ for $y \leq h$, Eq. (12) can be written

$$\omega = \frac{2 A_d \theta n_1 v_1}{3\pi^2 v_* v_2} \left(\frac{\sigma_*}{\tau}\right) \int_a^\infty \frac{\psi_2(y)}{y}\, dy \qquad (13)$$

where the dependence of the number of photons per second, ω , on the ratio σ_* / τ is shown explicitly.

Substituting from Eq. (8) for $\psi_2(y)$, the number of photons per second entering the detector is given by

$$\omega = \frac{2 A_d \theta n_1 v_1}{3\pi^2 v_* v_2} \left(\frac{\sigma_*}{\tau}\right) \psi_2(a)\, e^{a/\eta} \int_a^\infty \frac{1}{y} e^{-\frac{y}{\eta}}\, dy \qquad (14)$$

Putting $\xi = y/\eta$, Eq. (14) can be written in terms of a tabulated integral

$$\omega = \frac{2 A_d \theta n_1 v_1}{3\pi^2 v_* v_2} \left(\frac{\sigma_*}{\tau}\right) \psi_2(a)\, e^{a/\eta} \int_{a/\eta}^{\infty} \frac{1}{\xi} e^{-\xi} d\xi \qquad (15)$$

The total flux of target molecules at the surface of the lower plate, $\psi_2(a)$, can be expressed in terms of the probability, P , that an N_2 molecule will collide with a target molecule in traversing the maximum path length (diameter) in the target stream at $y = a$. Writing $n_2(y)$ for the density of target molecules, to an approximation consistent with Eq. (15), can be expressed as

$$\frac{P}{\sigma_0} = 2a \tan(\theta/2)\, n_2(a) \qquad (16)$$

And since

$$\psi_2(a) = \pi a^2 \tan^2(\theta/2)\, v_2\, n_2(a) \qquad (17)$$

this becomes

$$\psi_2(a) = \frac{\pi a v_2}{2} \left(\frac{P}{\sigma_0}\right) \tan(\theta/2) \qquad (18)$$

Finally, to the same approximation as Eq. (15), the total number of photons per second entering the detector is given by

$$\omega = \frac{A_d \theta^2 n_1 v_1 a}{6\pi v_*} \left(\frac{P}{\sigma_0}\right) \left(\frac{\sigma_*}{\tau}\right) e^{a/\eta} \int_{a/\eta}^{\infty} \frac{1}{\xi} e^{-\xi} d\xi \qquad (19)$$

which, when multiplied by the energy per photon becomes the wattage into the detector attributable to the excitation corresponding to σ_* .

The integral in Eq. (19) is plotted in Figure 15.

The values pertaining to the actual experiments are given below.

a = 2.54 cm

A_d = 0.0625 cm^2

n_1 = 2.75×10^{14} cm^{-3} for 5.8 Km/sec N_2 stream

= 1.86×10^{14} cm^{-3} for 4.3 Km/sec O stream

= 1.35×10^{14} cm^{-3} for 5.4 Km/sec Argon stream

$n_2(a)$ = 2.25×10^{14} cm^{-3} (for H_2O)

= 3.9×10^{14} cm^{-3} (for CO_2)

= 2.36×10^{14} cm^{-3} (for NH_3)

$\frac{P}{\sigma_o}$ = 0.31×10^{15} cm^{-2} (for H_2O)

= 0.53×10^{15} cm^{-2} (for CO_2)

= 0.32×10^{15} cm^{-2} (for NH_3)

v_1 = 5.8×10^5 cm/sec (for $N_2 - H_2O$, $N_2 - CO_2$, and $N_2 - NH_3$)

= 4.3×10^5 cm/sec (for $O - H_2O$)

= 5.4×10^5 cm/sec (for $Ar - H_2O$)

v_2 = 1.13×10^5 cm/sec (for H_2O)

= 5.4×10^4 cm/sec (for CO_2)

= 9.43×10^4 cm/sec (for NH_3)

v_* = 3.53×10^5 cm/sec (for $N_2 - H_2O$)

= 2.26×10^5 cm/sec (for $N_2 - CO_2$)

= 3.61×10^5 cm/sec (for $N_2 - NH_3$)

= 2.02×10^5 cm/sec (for $O - H_2O$)

= 3.70×10^5 cm/sec (for $Ar - H_2O$)

θ = 30° or 0.524 radians

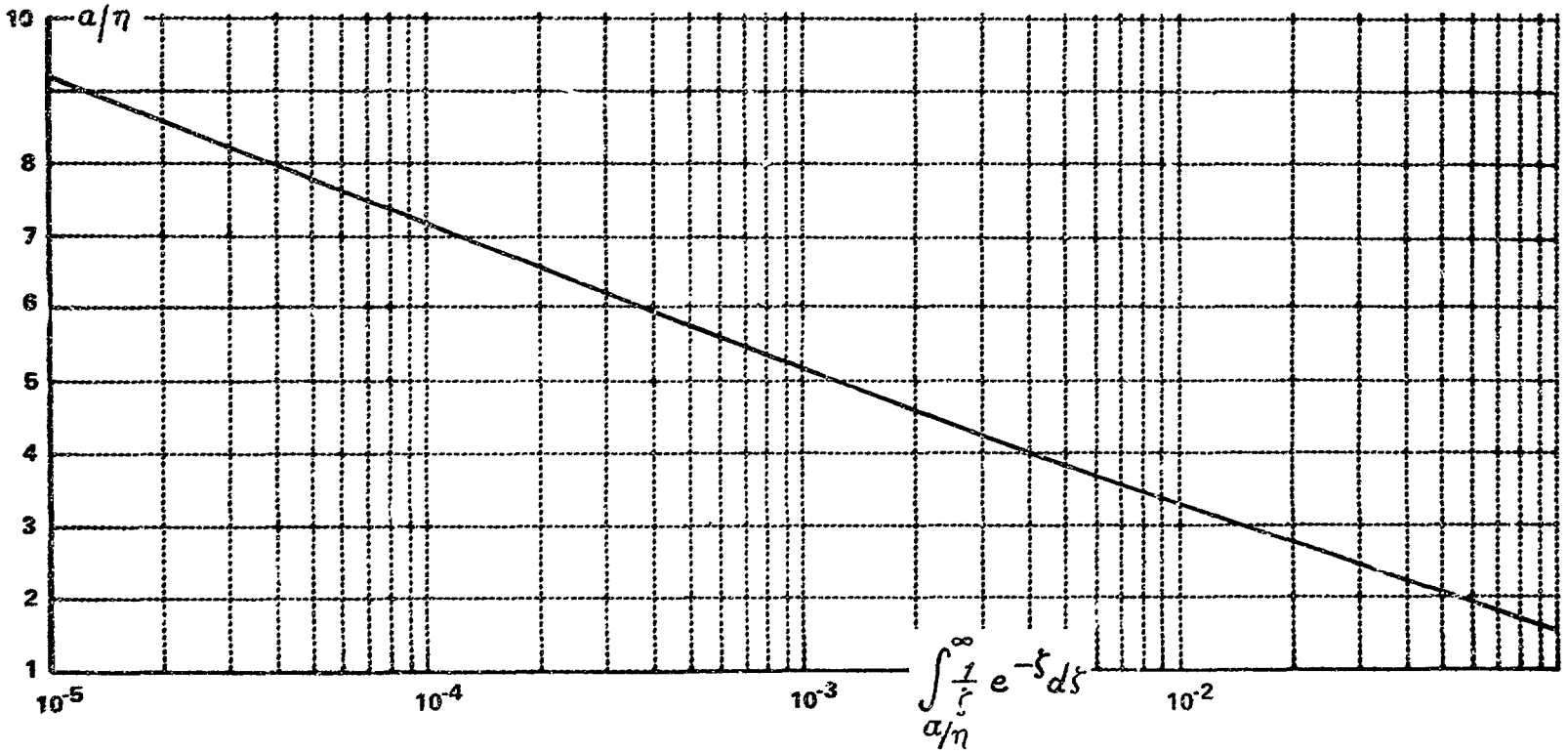

Figure 15 VALUES OF THE INTEGRAL OCCURRING IN EQUATIONS (8) AND (12)

$$\sigma_o = 3.22 \times 10^{-15} \quad \text{for } N_2 - H_2O$$
$$= 4.54 \times 10^{-15} \quad \text{for } N_2 - CO_2$$
$$= 1.7 \times 10^{-15} \quad \text{for } N_2 - NH_3$$
$$= 2.7 \times 10^{-15} \quad \text{for } O - H_2O$$
$$= 2.5 \times 10^{-15} \quad \text{for } Ar - H_2O$$

With these values, Eq. (19) can be used to express the experimental capability of measuring σ_* / τ in terms of the resolution of the detector.

$$\sigma_*/\tau = 3.842 \times 10^{-26} (\omega\tau) \quad (\text{for } N_2 - H_2O)$$
$$= 4.036 \times 10^{-26} (\omega\tau) \quad (\text{for } N_2 - CO_2)$$
$$= 2.710 \times 10^{-26} (\omega\tau) \quad (\text{for } N_2 - NH_3)$$
$$= 2.012 \times 10^{-26} (\omega\tau) \quad (\text{for } O - H_2O)$$
$$= 3.640 \times 10^{-26} (\omega\tau) \quad (\text{for } Ar - H_2O)$$

where $\omega\tau$ is in photons sec^{-1}.

The possibility of multiple collisions, which result in deexcitation of excited molecules, was a design consideration. This consideration leads to one of the design problems of the experiment which concerned the spacing of the target source and the detector. When operating with H_2O the source is water-jacketed at 100°F whereas the detector is at about 5°K and shielded at about 77°K. Therefore, adequate separation is necessary for thermal isolation. Also, in the flow between the plates, the cones of the target stream and of the field of view of the detector should not overlap up to a height beyond which essentially no excited states are produced. However, once a target molecule is highly excited, it moves with

the N_2 stream at a velocity $(v_1 - v_*)$ and its mean free path in the N_2 stream must be sufficient to ensure that collisional deexcitation will not interfere with the experiment. Thus the experiment was designed so that an excited molecule would have, on the average, about one collision before entering the detector field of view. The probability of deexcitation in a single collision is negligibly small.

The probability of the newly created excited particle undergoing a collision with a N_2 particle can be estimated on the basis of a typical gas-dynamic collision cross section, σ_o . In traveling between position x_1 where the excited particle is formed to position x_2 where it would radiate in the FOV of the detector, the probability of it striking a N_2 particle is given by

$$\frac{x_2 - x_1}{v_*} (v_1 - v_*) n_1 \sigma_o$$

The collision between the excited particle and a N_2 molecule is a much lower energy collision than the initial collision between a N_2 particle and a target gas molecule. The distance between the centerline of the FOV of the target gas, x_1 , and the centerline of the FOV of the detector, x_2 , was approximately 3.7 cm for our experiments. Thus if we assume a gas-dynamic collision cross section, σ_o , equal to 10^{-15} cm^2, then we can then estimate the probability of the excited target molecule undergoing a single collision with a N_2 particle in traveling the distance $x_2 - x_1$ as follows:

For H_2O $\left(\frac{x_2 - x_1}{v_*}\right)(v_1 - v_*)\frac{n_1}{\sigma_o}$ = 0.65

For CO_2 $\left(\frac{x_2 - x_1}{v_*}\right)(v_1 - v_*)\frac{n_1}{\sigma_o}$ = 1.6

For NH_3 $\left(\frac{x_2 - x_1}{v_*}\right)(v_1 - v_*)\frac{n_1}{\sigma_o}$ = 0.62

It thus appears that a negligible fraction of the excited target beam particles were deexcited prior to entering the FOV of the detector.

4. METHOD OF DATA ANALYSIS

Analysis of the data to determine the cross section for excitation has required an unfolding of the collisional excitation and radiative emission processes. For shortwave vibrational transitions most of the emission occurs in a relatively small spectral range, and can be clearly identified as radiation from a specific excited vibrational state. The cross section for excitation of this state can then be determined by multiplying the experimental value of σ_* / τ by the known radiative lifetime for the transition. In this way the cross section for H_2O (000-010) at 6.3 μm and NH_3 (ν_2) at 10.7 μm were determined. For the other transitions, however, where the observed radiation originates from a broad range of energy levels, or where only a portion of the band was observed (as with CO_2), a somewhat more detailed analysis is required. This analysis was applied to the pure rotational spectrum of water, but has not been completed for the CO_2 transitions. Thus partial cross sections are supplied for these excitations.

4.1 General Formulation

The cross section for excitation to the v, R vibrational-rotational state is taken as

$$\sigma_{vR} = P_v \, P_R \, \sigma_o \tag{20}$$

where P_v is a probability of excitation of a given vibrational state and P_R the probability of excitation of a given rotational state. For excitation to any given vibrational state v, the cross section is

$$\sigma_v = \sum_{\substack{all \\ R}} \sigma_{vR} = \sigma_o \, P_v \sum_{\substack{all \\ R}} P_R = \sigma_o \, P_v \tag{21}$$

where P_R is normalized so that

$$\sum_{\substack{all \\ R}} P_R = 1 \tag{22}$$

The intensity of the radiation that is observed immediately after collisional excitation is proportional to the ratio of the excitation cross section to the radiative lifetime, as previously discussed. Thus the parameter that can be measured for any transition j is

$$\bar{\theta}_j(\nu) = \frac{\sigma_{vR}}{\tau_j} = \sigma_{vR} A_j \tag{23}$$

where $A_j = \frac{1}{\tau_j}$ is the Einstein coefficient for spontaneous emission, and τ_j is the lifetime for transition j, originating from level $v R$. Combining Eqs. (21) and (23) for pure vibrational transitions permits the simple data reduction discussed above. In general, however, the filters employed transmit many spectral lines originating from considerably different energies, so that for each filter the observed radiation is proportional to the sum of all the terms $\theta_j(\nu)$ with values of ν within the passband. Then for each filter f

$$\frac{\sigma_*}{\tau}(f) = \sum_{j(f)} \theta_j(\nu) = \sum_{j(f)} (\sigma_{vR} A_j) \tag{24}$$

or

$$\frac{\sigma_*}{\tau}(f) = \sigma_o \sum_{j(f)} P_v P_R A_j \tag{25}$$

where $j(f)$ indicates all the spectral lines j passed by filter f. In these comparisons the kinetic cross section, σ_o, has been taken equal to 11.5×10^{-16} cm^2, consistent with the value used by Kolb, et al.[10] The radiative transition probabilities A_j have been taken from sources referenced below. It is the purpose of the experiments to determine values of P_v and P_R consistent with these assumptions.

Because of the large number of energy levels to which transitions can occur compared with the relatively few passbands in which observations are made, it is necessary to make some assumption about the values of P_R and P_v, and then adjust these assumptions to obtain a consistent

comparison with the data. To accomplish this, P_R is taken to depend only on the ratio of the energy of the rotational state to the center-of-mass energy of the collision. The energy dependence that is utilized is the calculated values obtained by Kolb et al.[10] for an impulsive rigid-rotor classical model of H_2O collisions with oxygen atoms. These values are shown in Figure 16, and are applied to the 5.8 Km/sec collision of N_2 and H_2O, where the value of E_{CM} is 15,400 cm, or 1.9 ev. With this model the probability of excitation into an energy range E to $E + \Delta E$ is equal to $\frac{P\Delta E}{E_{CM}}$ so that $P\left(\frac{E}{E_{CM}}\right)$ is normalized by the relation $\int_0^1 P\left(\frac{E}{E_{CM}}\right) d\left(\frac{E}{E_{CM}}\right) = 1$. In the present usage the probability of excitation into an energy level i is equal to P_{R_i} so that the normalization relation is $\sum_{i=1}^{i_{MAX}} P_{R_i} = 1$, where i represents the i^{th} energy level and i_{MAX} is the total number of rotational levels considered. Thus Kolb et al. values are related to those used here by

$$P_{R_i} = C\,P(E) \tag{26}$$

where C is a single proportionately constant determined from $\sum_{i=1}^{i_{MAX}} P_{R_i} = 1$. (Since the energy levels are distributed with reasonably constant density in the energy range of interest, C is approximately given by $C = 1/i_{MAX}$.)

4.2 H_2O Rotation

The pure rotational spectrum of H_2O extends over the entire 8-14 μm infrared region of interest, but the shorter wavelength radiation originates only from transitions between higher energy states. The energies of the rotational states and the wavelength and intensities of the transitions which originate from them have been calculated by Maki[11] and these calculations have been used in the present data reduction. There are $2J + 1$ energy states for each value of the rotational quantum number J, and their energies are spread between the limiting curves shown in Figure 17. These curves can be fit roughly to the form $E = BJ(J + 1)$, where

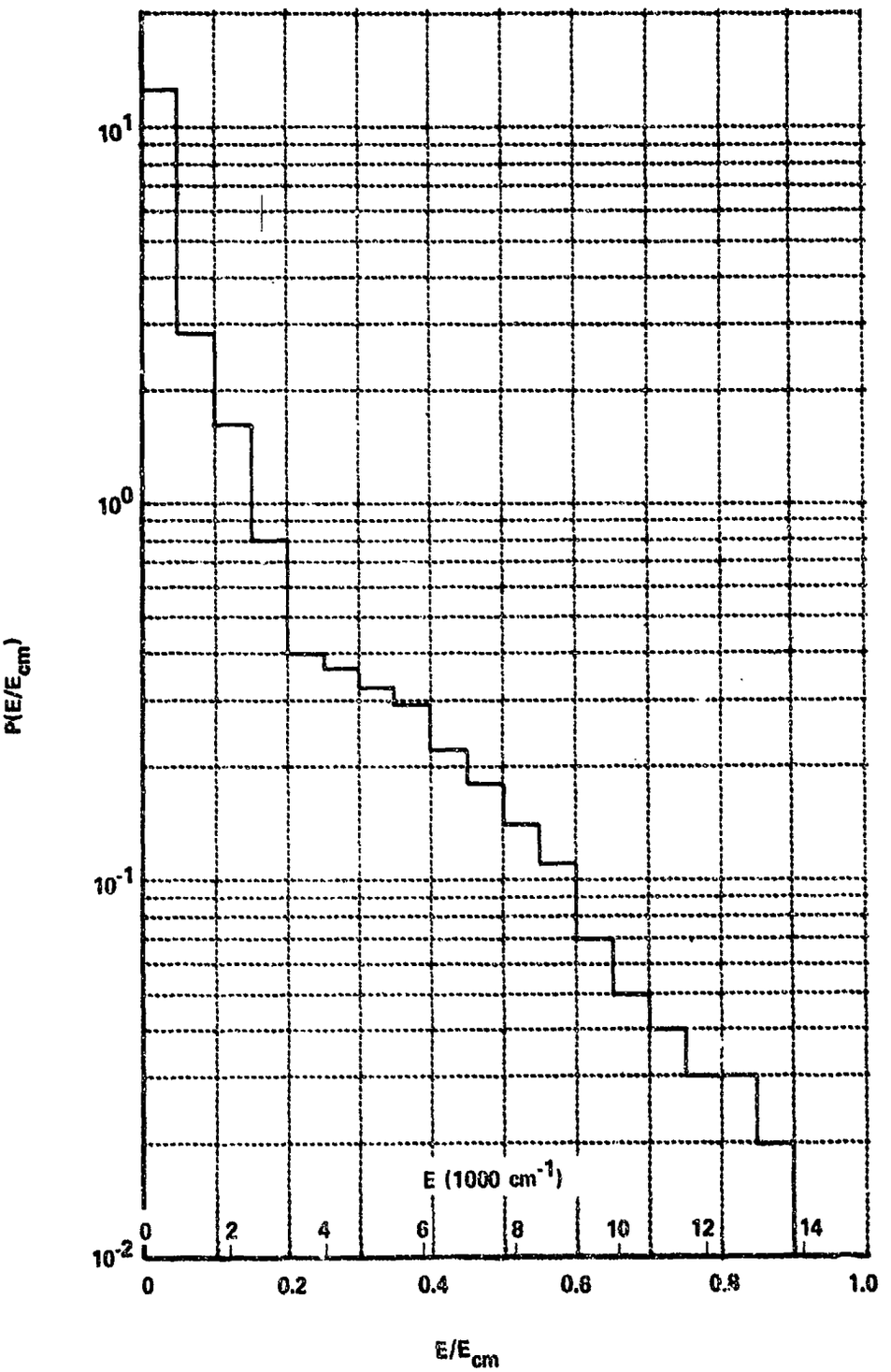

Figure 16 TRANSITION PROBABILITIES FOR ROTATIONAL EXCITATION OF H_2O, CALCULATED BY KOLB ET AL, REF. 10

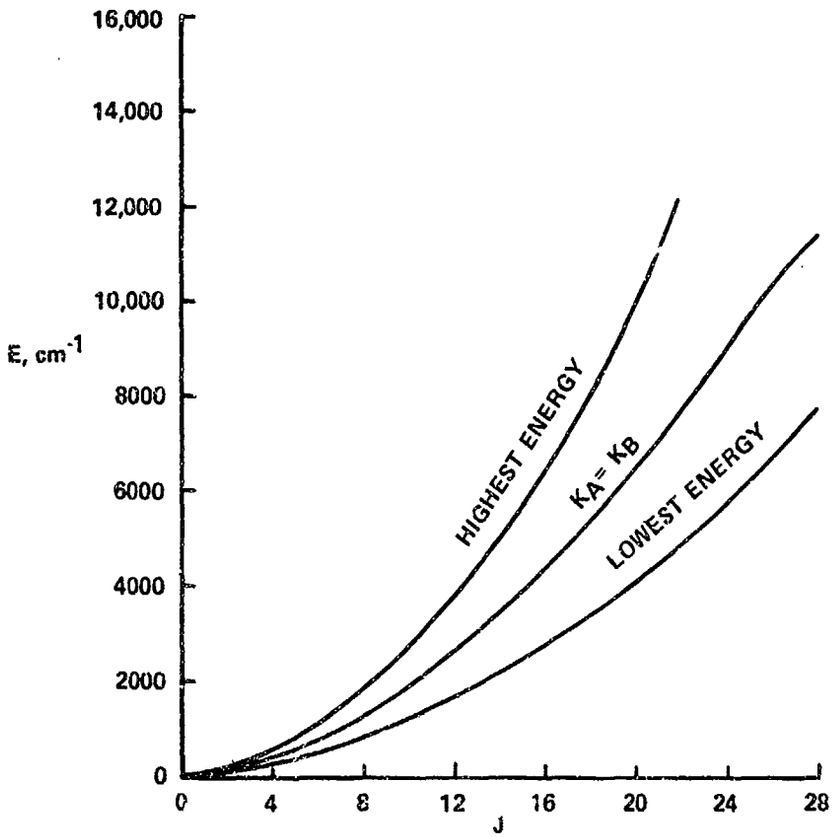

Figure 17 CALCULATED H_2O ENERGY LEVEL LIMITS

$B \approx 24\ cm^{-1}$ for the upper curve ($K^+ = J$) and $9.8\ cm^{-1}$ for the lower curve ($K^- = J$). Since transitions have $\Delta J = 1$, the wave number of the radiation that can be expected would vary roughly as $\nu = 2BJ$. This would imply, for example, that to obtain radiation of 14 μm wavelength or shorter ($\nu \gtrsim 700\ cm^{-1}$) would require excitation to energy levels of $J \gtrsim 16$ on the upper curve, or energies $> 5000\ cm^{-1}$. Detailed inspection of Maki's calculated data show that this is the case, as illustrated in Figure 13. In this figure, the Einstein A coefficients have been summed for the transitions in the interval $8.32 < \lambda < 14\ \mu m$ and the results plotted for $770\ cm^{-1}$ intervals of the upper energy state. It can be seen that very little radiation originates from energy levels below about $5000\ cm^{-1}$. At high energy levels the calculation becomes inaccurate; above about $13,000\ cm^{-1}$ some of the levels are not included. Fortunately at these high energies the probability of excitation is small, as shown in Figure 16. Thus the product of the curves in Figures 16 and 18, which supplies the radiation term in Eq. (21), decreases at high energy and it is not required to have an accurate value.

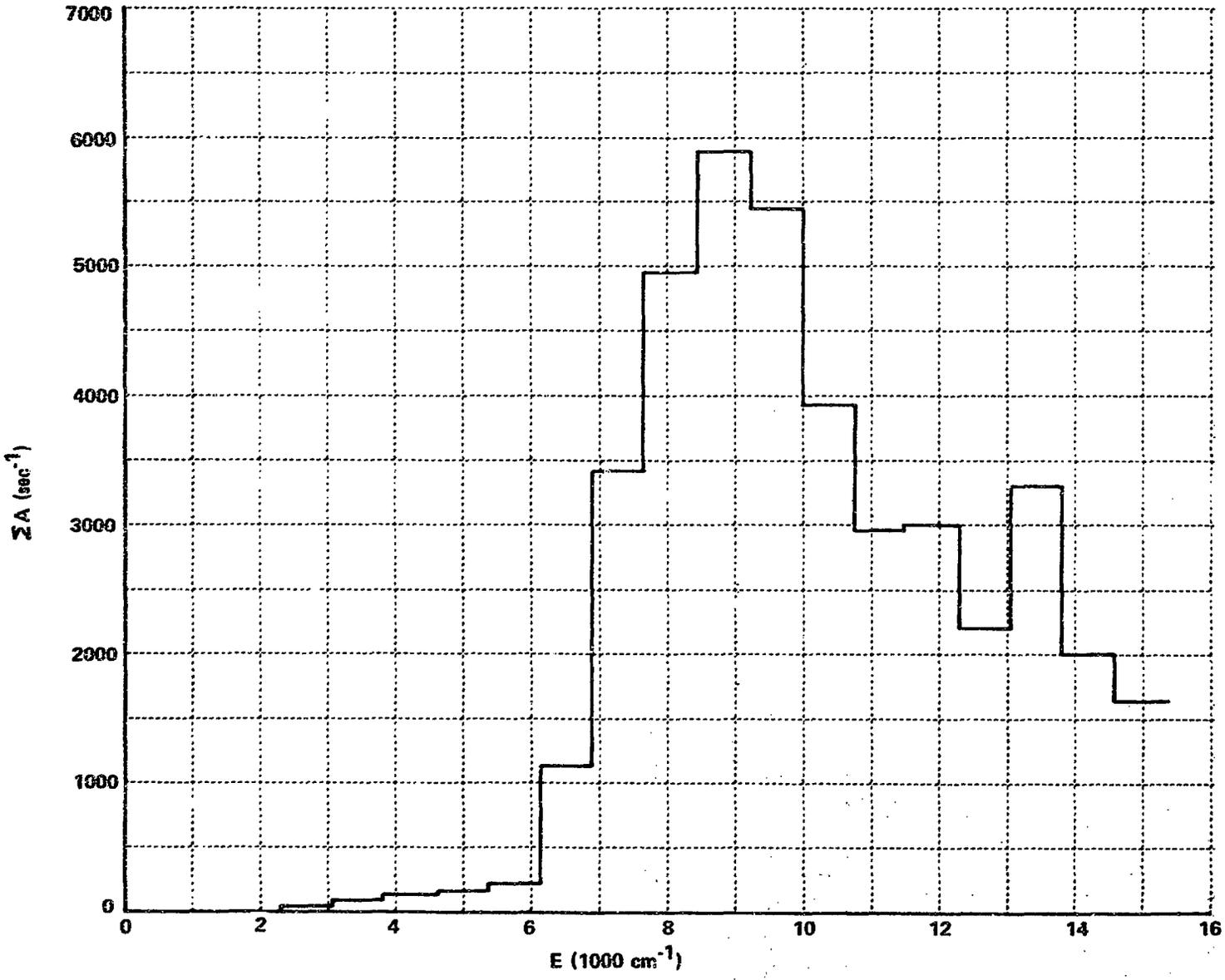

Figure 18 SUMMED EINSTEIN TRANSITION PROBABILITIES FOR STATES IN ENERGY INTERVALS CORRESPONDING TO THOSE SHOWN IN FIGURE 16, AND FOR RADIATION IN THE WAVELENGTH INTERVAL 8.32 - 14.0 μ

5. PRESENTATION OF EXPERIMENTAL DATA

5.1 N_2-H_2O Collisions at 5.8 Km/sec

The experimental results obtained for the infrared radiation from H_2O collisionally excited by N_2 at 5.8 Km/sec are given in Table I for all of the wavelength intervals studied in this work. Three important comments can be made about the results appearing in this table. First, the photon flux measured in the absence of H_2O injection for the 2.5 to 3.1 μm wavelength region was approximately equal to (6 percent greater) that measured with injection suggesting that the H_2O stretching mode was not excited. On the basis of experience with these measurements we feel that 10 percent effects can be resolved and that the slight decrease in signal observed at this wavelength with H_2O injection is not significant. The data reported in Table I for this wavelength suggest that the value of σ_* / τ must be less than 3.7×10^{-17} cm^2 sec^{-1}. Secondly, the magnitude of σ_* / τ measured in the 5.7 to 7.5 μm region is relatively large (0.46×10^{-15} cm^2 sec^{-1}), roughly the same as the value measured over the entire 8.3 to 14 μm region (0.35×10^{-15} cm^2 sec^{-1}). Finally, the sum of the σ_* / τ values measured at the 8.3 to 9.2, 9.1 to 10.3, 10.6 to 11.6, and 11.1 to 14.0 μm wavelength intervals is approximately equal to the value of σ_* / τ measured with the 8.3 to 14.0 μm filter, as would be expected.

Table I
EXPERIMENTAL RESULTS FOR N_2 - H_2O AT 5.8 km/sec

FILTER	NO H_2O INJECTION	WITH H_2O INJECTION	SIGNAL DUE TO H_2O	$(\sigma_* / \tau)_{EXP}$
microns	photons/sec	photons/sec	photons/sec	cm^2 sec^{-1}
2.5 TO 3.1	9.8×10^9	9.3×10^9	$< 0.95 \times 10^9$	$< 0.037 \times 10^{-15}$
5.7 TO 7.5	1.9×10^{10}	3.1×10^{10}	1.2×10^{10}	0.46×10^{-15}
8.3 TO 9.2	1.0×10^9	1.9×10^9	0.9×10^9	0.035×10^{-15}
9.1 TO 10.3	1.0×10^9	2.1×10^9	1.1×10^9	0.042×10^{-15}
10.6 TO 11.6	2.4×10^9	4.8×10^9	2.4×10^9	0.092×10^{-15}
11.1 TO 14.0	1.5×10^{10}	1.9×10^{10}	4.0×10^9	0.15×10^{-15}
8.3 TO 14.0	5.7×10^9	1.5×10^{10}	0.9×10^{10}	0.35×10^{-15}

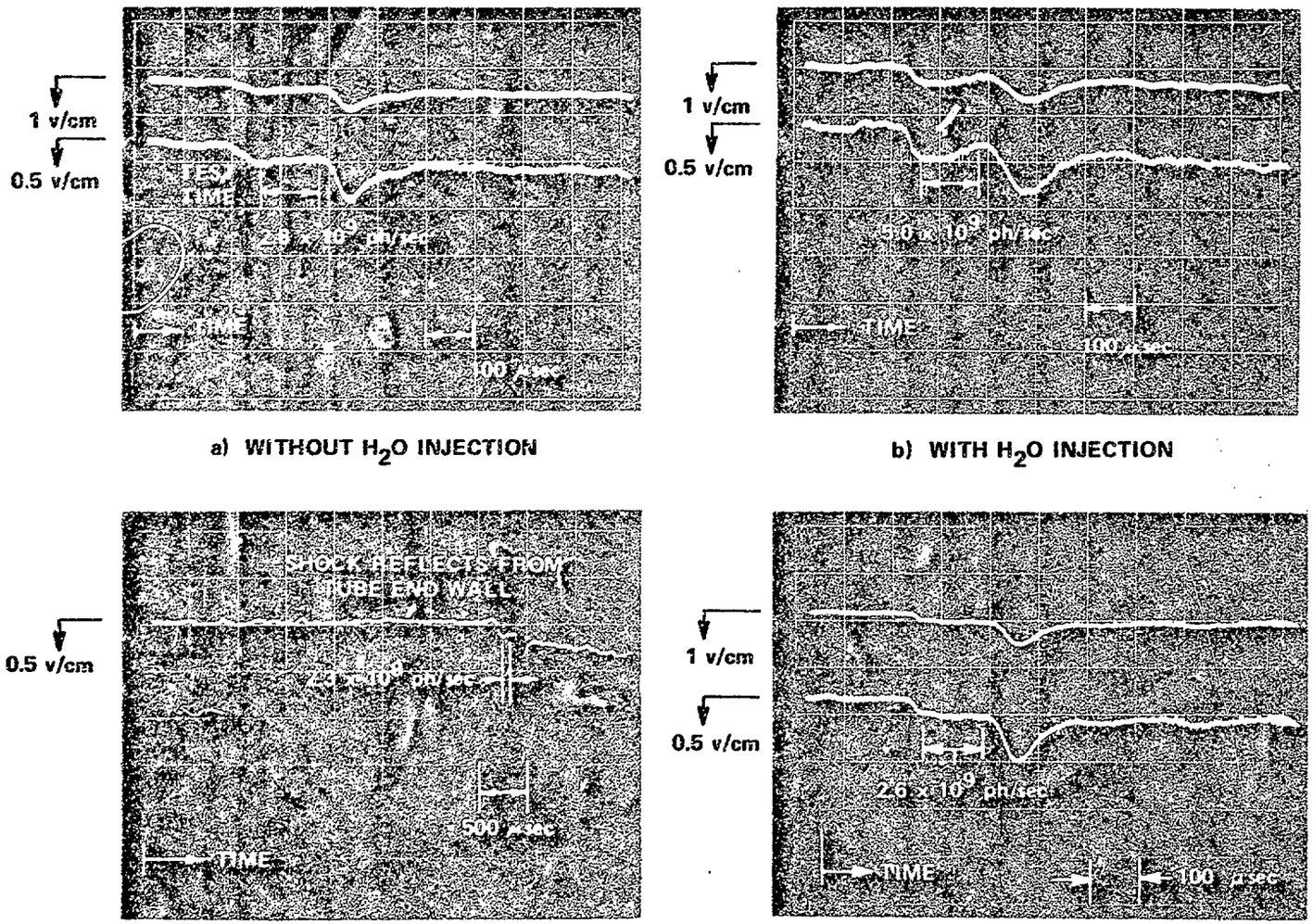

Figure 19 OSCILLOSCOPE RECORDS OBTAINED FOR 10.6 TO 11.6 MICRON FILTER FOR 5.8 KM/SEC N_2 PARTICLES

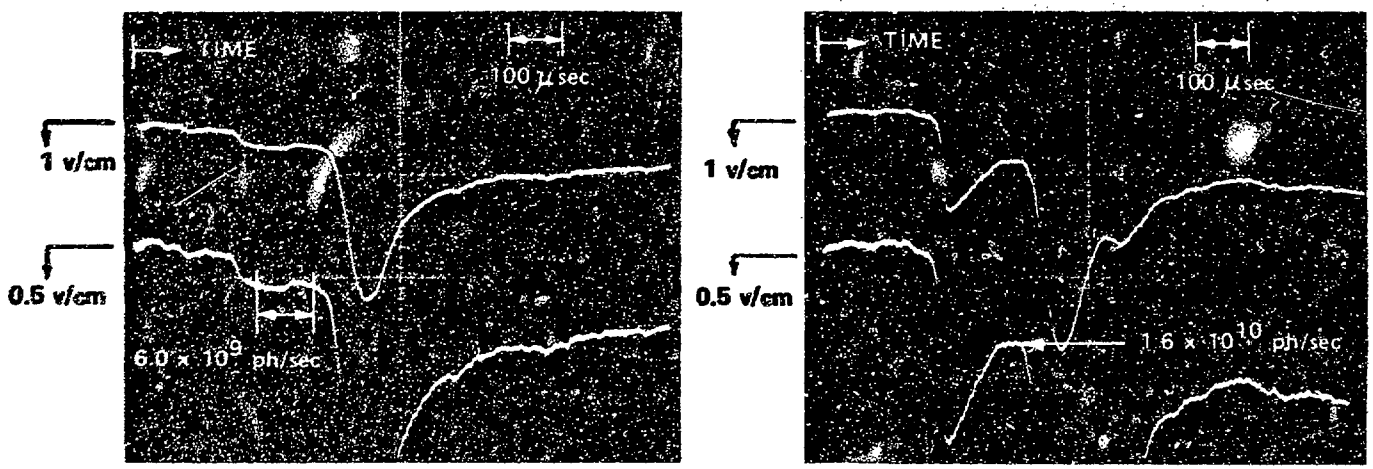

a) WITHOUT H_2O INJECTION

b) WITH H_2O INJECTION

Figure 20 OSCILLOSCOPE RECORDS OBTAINED FOR 8.3 TO 14.0 MICRON FILTER FOR 5.8 KM/SEC N_2 PARTICLES

Figure 19 is typical of the data obtained in these experiments. Figure 19(a) illustrates the detector-output history measured in the 10.6 to 11.6 μm wavelength region in the absence of H_2O injection. The test time is shown to be on the order of 100 μsec, consistent with the results presented in Section 2, and the photon flux is relatively uniform during this time period. Figure 19(b) was obtained for the same N_2 velocity but in this experiment H_2O was injected as a target gas. The photon flux measured during the test flow was almost a factor of two greater than that measured in the absence of H_2O injection.

Figure 19(c) is an oscilloscope record from a different "no injection" experiment, but this oscilloscope was triggered by a heat-transfer gauge located 20 inches downstream from the driver-tube diaphragm and the scope sweep speed was 500 μsec/cm instead of 100 μsec/cm as used on Figures 19(a), (b) and (d). The reason for showing this record is to illustrate that when the incident-shock reflects from the driven-tube end wall, creating the reservoir of high-enthalpy particles, the detector does not receive a signal from the shock tube that could potentially influence the results.

To be sure that the increased signal observed when H_2O was injected could in fact be attributed to the N_2-H_2O interaction, several experiments were performed in which argon was injected instead of H_2O. Figure 19(d) illustrates that when argon was injected the recorded detector output was found to be nearly identical to the signal received in the absence of injection.

Figure 20 is another illustration of the experimental data obtained with and without H_2O injection. These particular oscilloscope records were obtained using the 8.3 to 14.0 μm filter. Figure 20(a) illustrates that the photon flux measured in the absence of H_2O injection was 6.0×10^9 ph/sec as compared to the value of 1.6×10^{10} ph/sec shown in Figure 20(b) which was measured with H_2O injection. These results are included in the data summary presented in Table I and, as indicated there, result in a value of σ_* / τ equal to 0.35×10^{-15} cm^2 sec^{-1} for this wavelength region.

5.2 N_2-CO_2 Collisions at 5.8 Km/sec

The experimental results obtained for the infrared radiation from CO_2 collisionally excited by N_2 at 5.8 Km/sec are given in Table II for all of the wavelength intervals studied in this work. One additional filter appears in this table (4.28 to 4.34 μm) that was not used in the N_2-H_2O work. In addition, the 5.7 to 7.5 μm and the 11.1 to 14.0 μm filters were not used in the N_2-CO_2 studies. It was difficult to excite the 4.28 to 4.34 μm mode as illustrated by the oscilloscope records presented in Figur 21. The signal received by the detector with CO_2 injection was approximately 15 percent greater than that received without injection. For the wavelength intervals 8.3 to 9.2 μm, 9.1 to 10.3 μm, and 8.3 to 14.0 μm the signals recorded with injection were considerably greater than the background signals. However, in the 10.6 to 11.6 μm region the signals recorded with injection of CO_2 were less than 10 percent greater than those recorded in the absence of injection so that only an upper limit of the value for σ_* / τ could be determined at this wavelength interval.

Table II
EXPERIMENTAL RESULTS FOR N_2 - CO_2 AT 5.8 km/sec

FILTER	NO CO_2 INJECTION	WITH CO_2 INJECTION	SIGNAL DUE TO CO_2	$(\sigma_* / \tau)_{EXP}$
microns	photons/sec	photons/sec	photons/sec	$cm^2\ sec^{-1}$
4.28 TO 4.34	7.8×10^8	9.5×10^8	0.17×10^9	0.007×10^{-15}
8.3 TO 9.2	1.0×10^9	1.3×10^9	0.3×10^9	0.012×10^{-15}
9.1 TO 10.3	1.0×10^9	1.5×10^9	0.5×10^9	0.020×10^{-15}
10.6 TO 11.6	1.6×10^9	1.7×10^9	0.1×10^9	0.004×10^{-15}
8.3 TO 14.0	5.7×10^9	1.6×10^{10}	1.0×10^{10}	0.40×10^{-15}

5.3 N_2-NH_3 Collisions at 5.8 Km/sec

Table III presents a summary of the values for σ_* / τ obtained for N_2 particles at 5.8 Km/sec interacting with NH_3. The three wavelength intervals that were studied for this combination of gases were 8.3 to 9.2 μm, 10.6 to 11.6 μm, and 8.3 to 14.0 μm. Even though all of the available filters were not used in this study, the results presented in Table III suggest that the value of σ_* / τ measured for the 8.3 to 14.0 μm wavelength region is consistent with the values measured in the two intermediate wavelength intervals.

Reproduced from
best available copy.

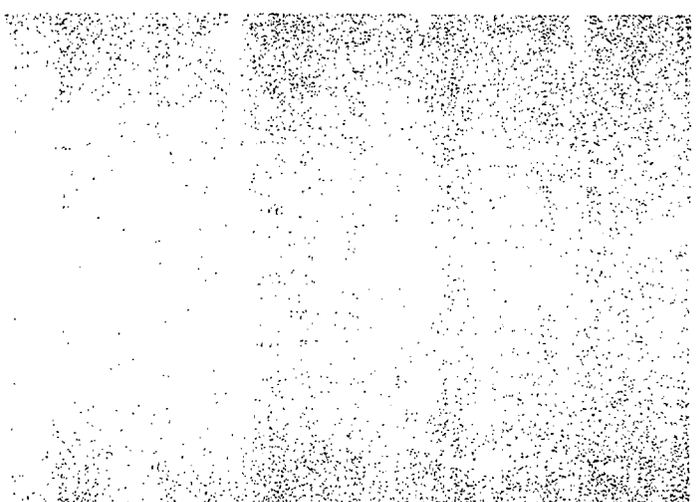

a) WITHOUT INJECTION

b) WITH CO_2 INJECTION

Figure 21 OSCILLOSCOPE RECORDS OBTAINED FOR 4.28 TO 4.34 MICRON FILTER FOR 5.8 KM/SEC N_2 PARTICLES

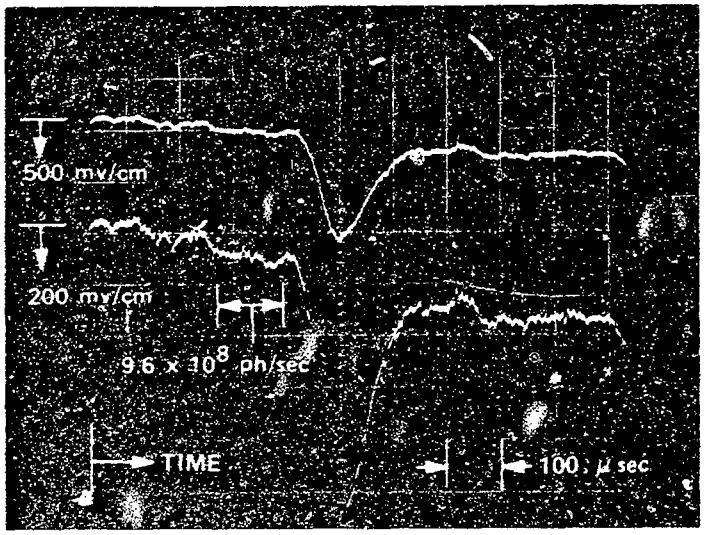

a) WITHOUT INJECTION

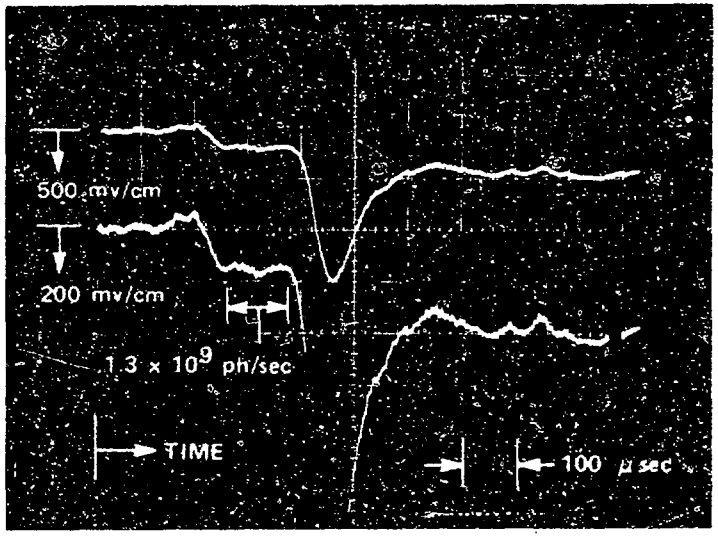

b) WITH CO_2 INJECTION

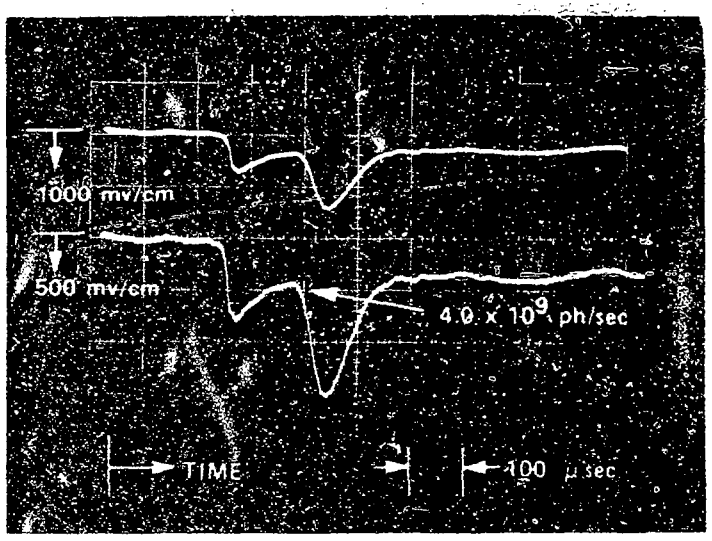

c) WITH NH_3 INJECTION

Figure 22 OSCILLOSCOPE RECORDS OBTAINED FOR 8.3 TO 9.2 MICRON FILTER FOR 5.8 KM/SEC N_2 PARTICLES

Table III

EXPERIMENTAL RESULTS FOR N_2 - NH_3 AT 5.8 km/sec

FILTER	NO NH_3 INJECTION	WITH NH_3 INJECTION	SIGNAL DUE TO NH_3	$(\sigma_*/\tau)_{EXP}$
microns	photons/sec	photons/sec	photons/sec	$cm^2\ sec^{-1}$
8.3 TO 9.2	1.0×10^9	3.9×10^9	2.9×10^9	0.079×10^{-15}
10.6 TO 11.6	1.6×10^9	6.6×10^9	5.0×10^9	0.14×10^{-15}
8.3 TO 14.0	5.7×10^9	2.5×10^{10}	1.9×10^{10}	0.51×10^{-15}

Figure 22 illustrates the characteristics of the oscilloscope records obtained with CO_2 injection or NH_3 injection in the 8.3 to 9.2 μm wavelength region (note the sensitivity change on Figure 22(c)). The photon flux recorded in the absence of injection was approximately 9.6×10^8 ph/sec as illustrated by Figure 22(a). When CO_2 was injected, the photon flux increased to 1.3×10^9 ph/sec and the resulting σ_* / τ was deduced to be 0.0028×10^{-15} cm^2 sec^{-1}. However, when NH_3 was injected, the photon flux increased to 4.0×10^9 ph/sec and the value of σ_* / τ was determined to be 0.045×10^{-15} cm^2 sec^{-1}.

Comparison of Tables I, II and III suggests that the values of σ_* / τ measured at selected wavelength intervals for N_2-NH_3 collisions were always greater than corresponding values measured for either the N_2-H_2O or N_2-CO_2 interactions. However, the N_2-CO_2 radiation in the 11.6 to 14 μm (i.e. near the 15 μm bending of CO_2) is probably greater than that for H_2O or NH_3. It can further be noted that the values of σ_* / τ measured at specified wavelength intervals for the N_2-H_2O interactions were always greater than corresponding values measured for N_2-CO_2 interactions.

The spectral nature of the results is demonstrated in Figures 23 to 25. On each graph the quantity $\frac{\sigma_* / \tau}{\Delta \lambda}$ is plotted vs wavelength, and is compared with the optical absorption coefficient for the target gas. The shape of the absorption coefficients used were those for 300° gas. The

purpose of the comparison is to demonstrate the correlation between the measured radiation and the spectral features of the gas, thus confirming that the source of radiation is the species being introduced through the target beam.

In Figure 23 the absorption of the bending mode of water occurs at 6.3 μm. The rotational spectrum observed at long wavelength does not appear in the cold absorption spectrum, since it results from transitions between very high-energy levels; analysis of these transitions is discussed in the following section. As indicated in Table IV, most of the contribution from the 5.7 to 7.5 μm filter and some from the 8.3 to 9.2 μm filter were used to determine σ_* for the 010 transition.

In Figure 24 the absorption curve of CO_2 is shown, the prominent features being the 4.3 μ asymmetric stretch and the 15 μ bending mode. The five measurements of $(\sigma_*/\tau)/\Delta\lambda$ are also shown. The measurement from 8.3 to 14 μm, corrected for the small contributions from 8.3 to 11.6, is plotted in the region 11.6 - 14 μm. It can be inferred from these figures that the measurement of $\frac{\sigma_*}{\tau}$ for both of these bands supply only partial measurements of σ_* for the (001) and (010) excitation cross sections.

In Figure 25 the overall measurement of σ_*/τ from 8 to 14 μm has been used to normalize the scale of the curve. The separate measurements in the spectral regions 8.3 - 9.2 μm and 10.6 - 11.6 μm are then plotted in their spectral regions and it is seen that they are consistent with the broad-band measurement. It is expected that the overall measurement from 8 - 14 μm supplies a good total cross section for excitation of the ν_2 mode.

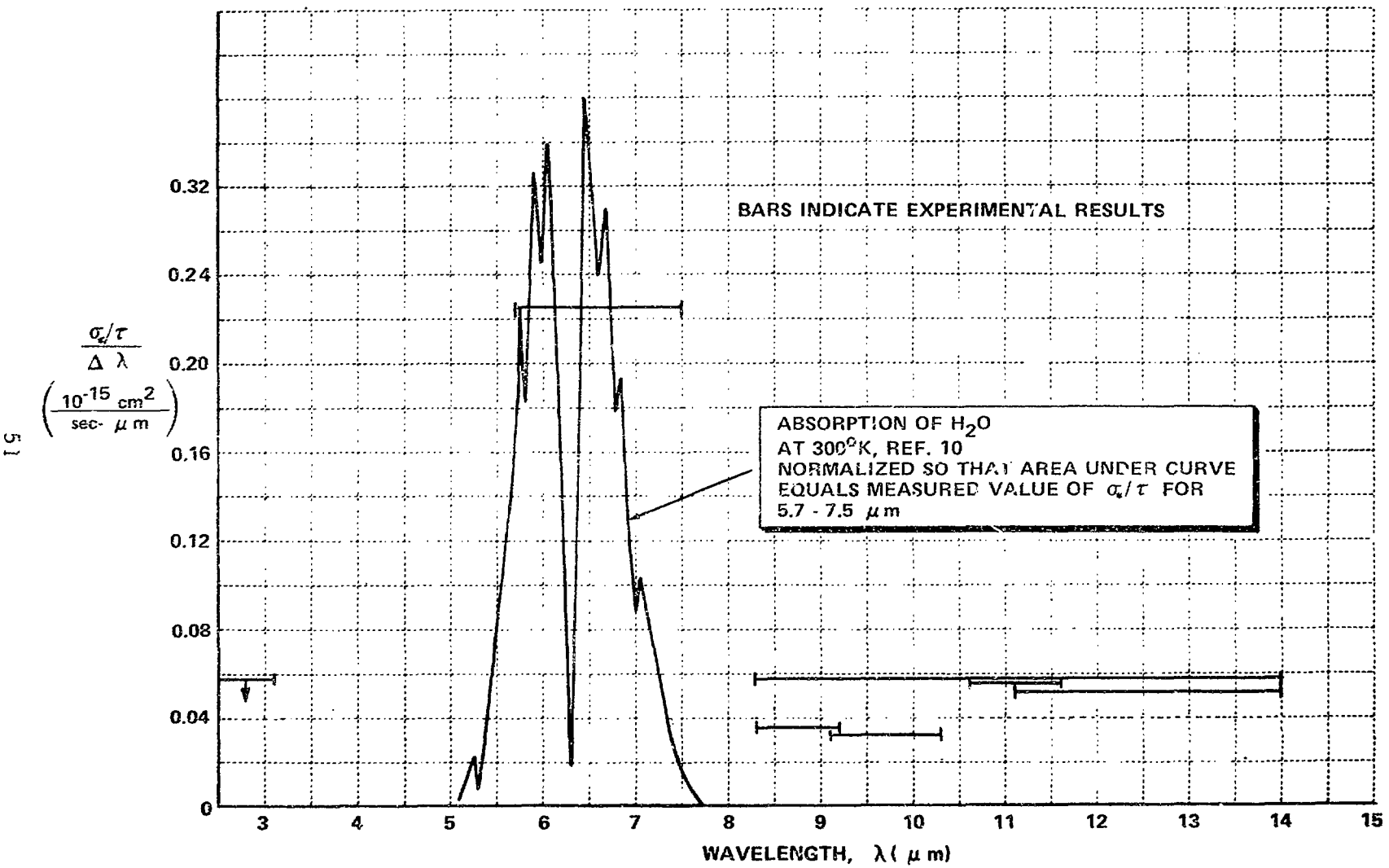

Figure 23 SPECTRAL DEPENDENCE OF COLLISIONALLY INDUCED RADIATION WITH H_2O-N_2 AT 5.8 KM/SEC

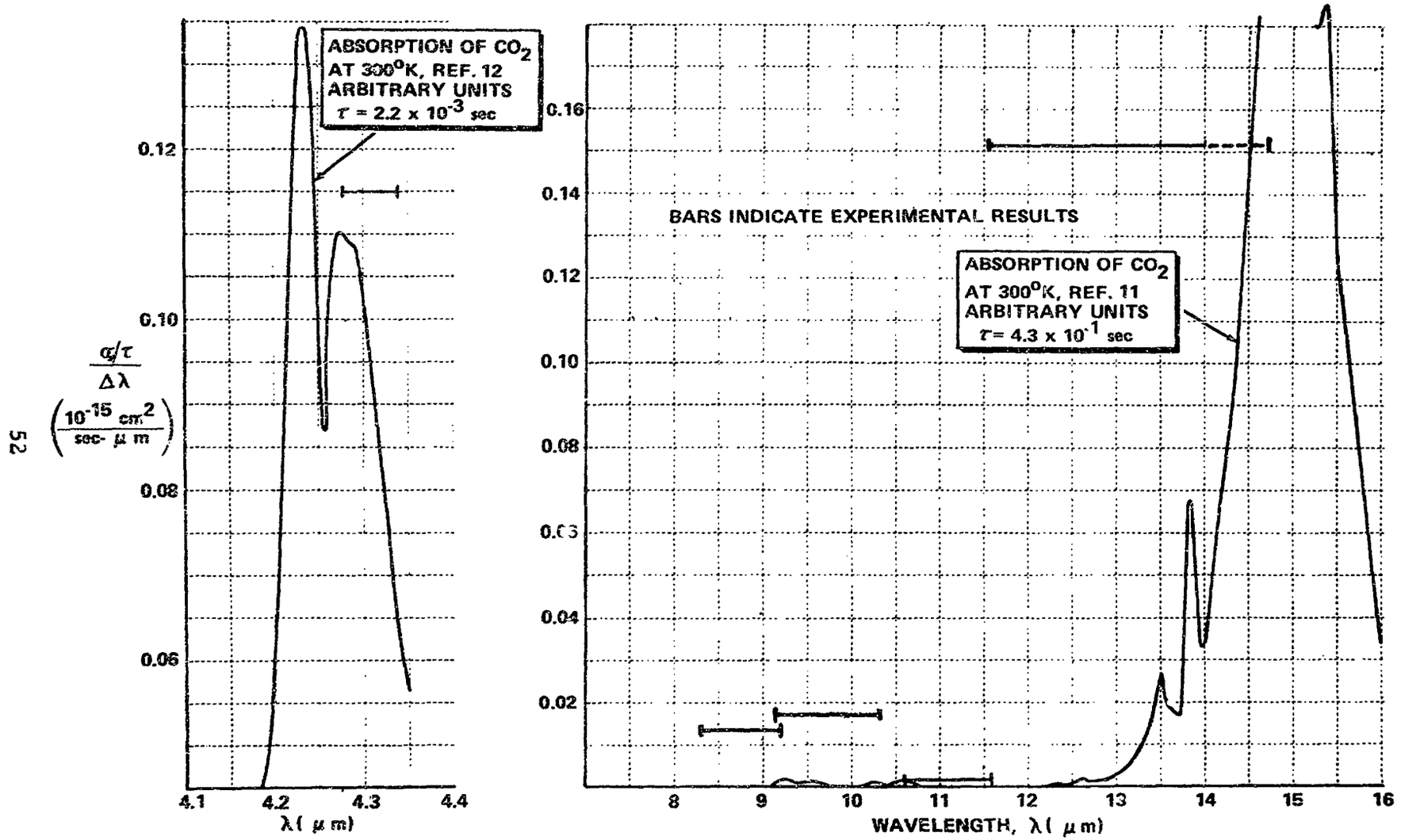

Figure 24 SPECTRAL DEPENDENCE OF COLLISIONALLY INDUCED RADIATION WITH CO_2-N_2 AT 5.8 KM/SEC

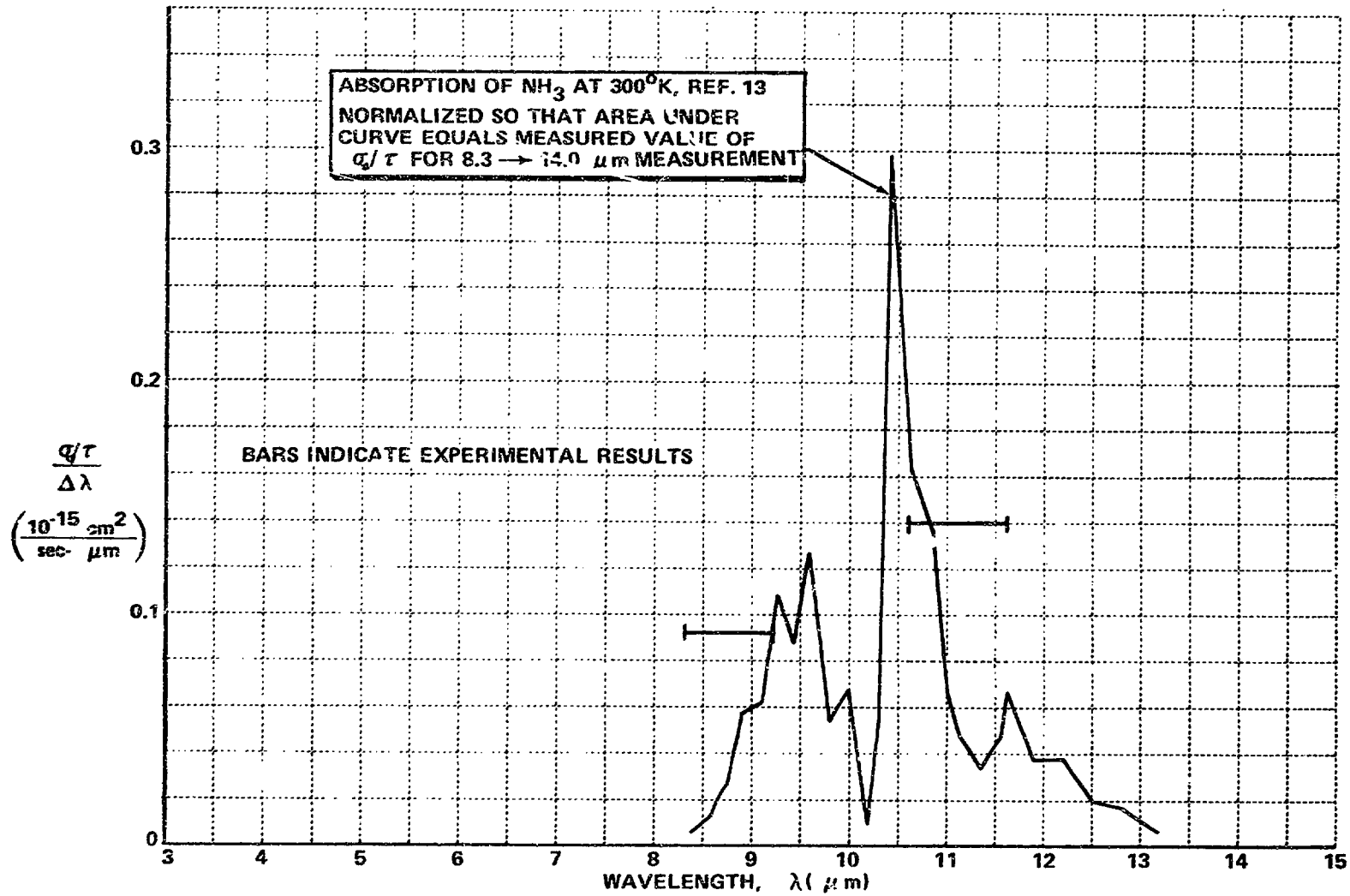

Figure 25 SPECTRAL DEPENDENCE OF COLLISIONALLY INDUCED RADIATION WITH NH_3-N_2 AT 5.8 KM/SEC

Table IV

COMPARISON OF EXPERIMENTAL RESULTS WITH CALCULATIONS FOR $N_2 - H_2O$ AT 5.8 km/sec

ENERGY INTERVAL cm^{-1}	$\left(\frac{\sigma_x}{\gamma}\right)\Delta E^{(f)}$ $cm^2 sec^{-1} \times 10^{18}$					
	5.67-7.45 μm	8.29-9.23 μm	9.13-1033 μm	10.61-11.57 μm	11.05-14 μm	8.32-14 μm
0-770	0	0	0	0	0	0
770-1541	0	0	0	0	0	0
1541-2312	0	0	0	0	0.37	0.37
2312-3083	0	0	0	0.33	10.97	11.01
3083-3853	0	0	0.12	2.03	28.90	31.10
3853-4624	0	0.0018	2.16	7.34	35.27	48.17
4624-5395	0	2.11	6.41	10.90	30.68	54.10
5395-6166	0	6.30	11.62	21.60	31.00	66.03
6166-6936	0	9.56	14.28	22.41	232.57	281.28
6936-7707	1.37	12.03	32.20	4.94	673.30	710.86
7707-8478	1.24	9.48	21.74	12.55	767.74	802.82
8478-9249	7.30	13.35	252.53	10.11	477.40	748.55
9249-10019	25.81	4.72	161.86	1.06	273.00	442.65
10019-10790	30.49	2.08	89.59	50.58	130.63	221.49
10790-11561	.76	0.95	31.33	33.02	84.46	137.16
11561-12332	53.65	.08	14.80	18.49	40.56	103.93
12332-13105	30.08	.21	17.41	49.98	26.31	75.39
13105-13873	106.48	19.13	9.18	21.27	9.39	76.07
13873-14644	0	0	0	0	0	0
14644-15415	0	0	0	0	0	0
$(\sigma_x/\gamma)_{calc}^{(f)}$	257.18	80.00	665.23	266.61	2852.55	3810.98
$(\sigma_x/\gamma)_{exp}$	160	13	15	21	54	120
(1/50) $(\sigma_x/\gamma)_{calc}$	5	1.6	13	5.3	57	76

5.4 Rotational Data for N_2 - H_2O Collisions

The ratio of excitation cross section to radiative lifetime for the pure rotational spectrum of H_2O was calculated as described in Section 4. The numerical results obtained for $(\sigma_*/\tau)(f)$ (Eq. (24)) for each energy interval and for each filter is shown in Table IV. The sum of these values over all energy intervals then supplies the value of $(\sigma_*/\tau)(f)$ to compare with experimental results, $(\sigma_*/\tau)_{exp}$. For this comparison, which is shown in TableIV, a value of $\sigma_* = 1.0 \times 10^{-15}$ cm^2 was used to reduce the experimental data in order to be consistent with the calculation. For this reason, the results (σ_*/τ) of Table V and those of Table I are different. It can be seen that the calculated values σ_*/τ are about 50 times too large at the long wavelengths, where there should be no interference from vibration-rotation transitions. In the third summary line of Table I the calculated value is shown reduced by a factor of 50. This brings the longer wavelengths into reasonable agreement, and the additional radiation at the short wavelength is attributable to the 010-000 vibrational-rotational transition. There is an unexplained discrepancy for the 10.61 μ - 11.57 μ filter, where the low calculated value reflects the unusually small number of strong lines attributed to this wavelength region.

5.5 Vibrational Data for N_2 - H_2O Collisions

The short wavelength radiation at 5.67 - 7.45 μ has been attributed to the 000-010 vibrational rotational transitions. Using a lifetime of $\tau = 4.5 \times 10^{-2}$ sec,[12] we obtain $\sigma_* = 2.1 \times 10^{-17}$ cm^2. A measurement in the wavelength interval 2.5 - 3.1 μ did not yield a measurable signal, and from this it was concluded that the cross section for the transition 000-001 is less than 9.3×10^{-19} cm^2. These data are summarized in Table V.

Table V
CROSS SECTIONS FOR VIBRATIONAL EXCITATION IN COLLISIONS WITH N_2 AT 5.8 km/sec

	$\Delta\lambda$ μm	τ sec	$(\sigma^*/\tau)_{EXPT.}$ $cm^2\ sec^{-1}$	$\sigma^*(\Delta\lambda)$ cm^2
H_2O 000-010	5.7 - 7.5	4.5×10^{-2}	0.46×10^{-15}	2.0×10^{-17}
000-001	2.5 - 3.1	2.5×10^{-2}	$< 0.037 \times 10^{-15}$	$< 9.3 \times 10^{-19}$
CO_2 000-010	11.6 - 14	4.3×10^{-1}	0.36×10^{-15}	1.6×10^{-16} (partial)
000-001	4.28 - 4.34	2.2×10^{-3}	0.007×10^{-15}	1.5×10^{-20} (partial)
NH_3 0000-0100	8.3 - 14	6.8×10^{-2}	0.51×10^{-15}	3.5×10^{-17}

5.6 Vibrational Data for CO_2 and NH_3 Excited by N_2 Collisions

A measurement of CO_2 radiation with a narrow-band filter at 4.28 - 4.34 μ yields a partial cross section for excitation of (001) of CO_2 of 1.54×10^{-20} cm^2. This low value is associated with the narrow passband, as seen on Figure 24. It is expected that measurement of all the radiation from this band would yield a cross section several times larger.

As seen in Table II and Figure 24, most of the CO_2 radiation measured in the long wavelength region is contained in the 11.5 to 14.0 μm region. The wavelength of detector cut-off is nominally 14.0 μm at which point the sensitivity has decreased to 0.24 of maximum sensitivity. At 14.5 μm the sensitivity has decreased to 0.1 of the 14.0 μm value and at 14.75 μm it has decreased to 0.05 of the 14.0 μm value.* In Figure 24 it is seen that the CO_2 transition probability increases by a factor of approximately 5 in the 14.0 to 14.5 μm interval and by a factor of approximately 10 in the 14.0 to 14.75 μm interval. It is probable that in these experiments a significant portion of the CO_2 radiation in the 14.0 to 14.75 μm region was received by the detector. For this reason, a dotted line has been used to represent that portion of the experimental result on Figure 24 that extends beyond nominal detector cut-off.

* Data supplied by Santa Barbara Research Corporation for the material from which this detector was cut.

The experimental determination of σ_*, shown in Table V to be 0.16×10^{-15} cm^2, would be expected to represent a fraction of the total cross section, but it is difficult to estimate the magnitude of this fraction. A recent calculation by R. Marriott (unpublished)** gives a value of $\sigma_* = 0.155 \times 10^{-15}$ cm^2 for collision at a relative velocity of 5.3 Km/sec.

The NH_3-N_2 measurement utilized a filter which passed 8.3 - 14 μ. Separate measurements were made in the wavelength intervals 8.3 to 9.2 μm and 10.6 to 11.6 μm as shown in Table III. It is illustrated on Figure 24 that the radiation of interest is centered at about 10.4 μm so that the measurements from 8 - 14 μ should encompass the entire band. Thus the value of $\sigma_* = 3.5 \times 10^{-17}$ should properly represent the cross section for exciting the ν_2 mode.

5.7 O - H_2O Collisions at 4.3 Km/sec

The experimental results obtained for the infrared radiation from H_2O collisionally excited by O atoms at 4.3 Km/sec are given in Table VI for the wavelength intervals 2.46 to 3.13 μm, 5.67 to 7.45 μm and 11.1 to 14.0 μm. It is difficult to directly compare these results with the N_2 - H_2O results given in Table I because of the significant difference (4.3 Km/sec vs. 5.8 Km/sec) in the O and N_2 particle velocities. The reason that these particle velocities are not the same is that helium instead of hydrogen was used as the driver gas for the O - H_2O experiments because it was found that the H_2 - O_2 interaction in the reflected-shock reservoir and in the nozzle expansion significantly complicated interpretation of the results.

Table VI
EXPERIMENTAL RESULTS FOR O - H_2O AT 4.3 km/sec

FILTER	NO H_2O INJECTION	WITH H_2O INJECTION	SIGNAL DUE TO H_2O	$(\sigma_*/\tau)_{EXPT.}$
microns	photons/sec	photons/sec	photons/sec	cm^2 sec^{-1}
2.46 TO 3.13	4.4×10^9	6.0×10^9	1.6×10^9	0.03×10^{-15}
5.67 TO 7.45	9.5×10^9	15.0×10^9	5.5×10^9	0.11×10^{-15}
11.1 TO 14.0	5.2×10^9	9.5×10^9	4.3×10^9	0.09×10^{-15}

** Private Communication: R. Marriott, Research Institute for Engineering Sciences, Wayne State Univ., Detroit, Michigan.

Figure 26 is typical of the oscilloscope records obtained in the oxygen experiments. The detector-output history in the absence of H_2O injection is shown in Fig. 4(a) for the 2.46 to 3.13 μm filter and Fig. 4(b) illustrates the data record obtained with H_2O injection. The test time is marked on both of these records and shown to be approximately 160 microseconds which is consistent with previous measurements mentioned in Section 2. The photon flux measured in the absence of injection is shown to be 3.9×10^9 ph/sec as compared to 6.6×10^9 ph/sec with injection. The difference between these signals is used to compute a value for σ_* / τ equal to 0.03×10^{-15} cm^2 sec^{-1}.

5.8 Rotational Data for $O - H_2O$ Collisions

The ratio of the excitation cross section to radiative lifetime for the pure rotational spectrum of H_2O was calculated for the oxygen experiments using the technique described in Section 4. Numerical results similar to those shown in Table V were obtained for each energy interval for the 11.1 to 14.0 μm filter. These values were summed over all energy intervals to arrive at a value of $(\sigma_* / \tau)_{CALC}$ which was approximately 1.18 times greater than the measured value $(\sigma_* / \tau)_{EXPT}$. The agreement between experiment and calculation is considerably better than was obtained for the $N_2 - H_2O$ experiments discussed in Section 5.4 but this is not surprising since the theoretical model was formulated for the case of H_2O collisions with oxygen atoms.

5.9 Vibrational Data for $O - H_2O$ Collisions

Table VII summarizes the short-wavelength radiation measurements obtained for the $O - H_2O$ experiments. The 2.46 to 3.13 μm radiation has been attributed to the 000-001 H_2O stretching mode and the 5.67 to 7.45 μm radiation has been attributed to the 000-010 bending mode. Using radiative lifetimes of 2.5×10^{-2} sec and 4.5×10^{-2} sec, respectively, the excitation cross sections deduced from the experimental data are 7.5×10^{-19} cm^2 sec^{-1} (2.46 to 3.13 μm) and 5.0×10^{-18} cm^2 sec^{-1} (5.67 to 7.45 μm).

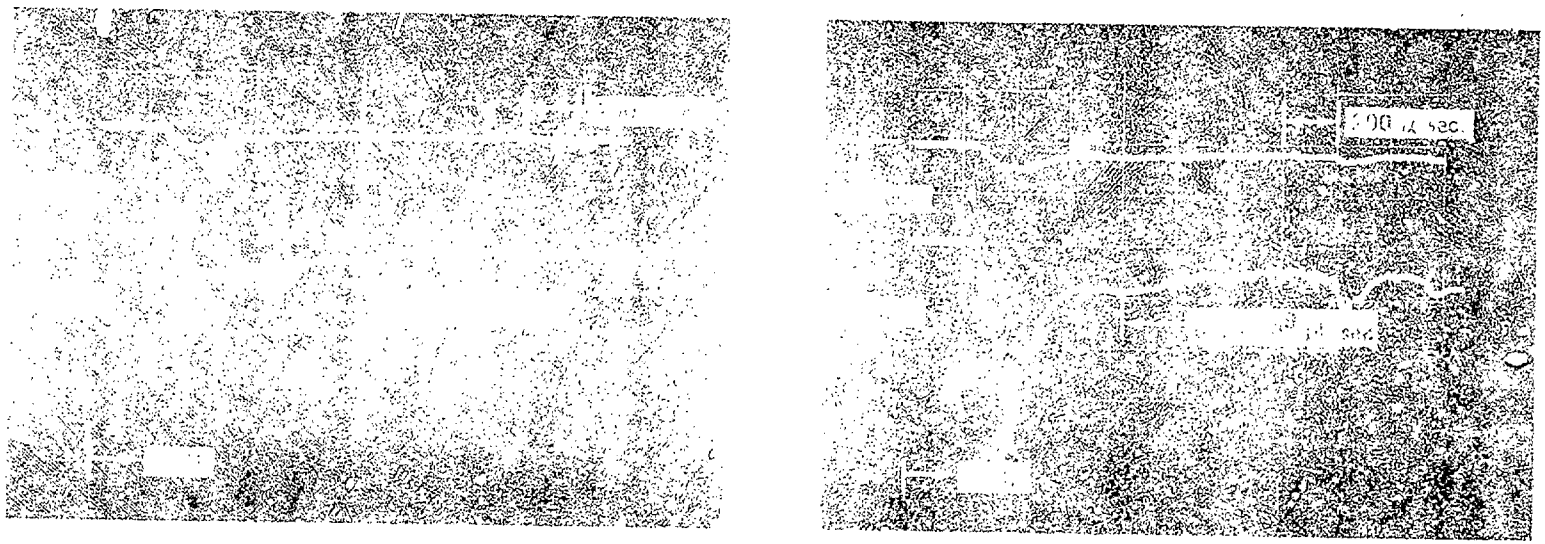

a) WITHOUT H_2O INJECTION

b) WITH H_2O INJECTION

Figure 2 6 OSCILLOSCOPE RECORDS OBTAINED FOR 2.46 TO 3.13 MICRON FILTER FOR 4.3 km/sec 0 ATOM PARTICLES

Table VII
CROSS SECTIONS FOR VIBRATIONAL EXCITATION OF H_2O IN COLLISIONS WITH 0 ATOMS AT 4.3 km/sec

		$\Delta\lambda$	τ	$(\sigma_*/\tau)_{EXPT.}$	$\sigma_*(\Delta\lambda)$
		microns	sec	$cm^2\ sec^{-1}$	cm^2
H_2O	000-010	5.67 TO 7.45	4.5×10^{-2}	$0.1,1 \times 10^{-15}$	5.0×10^{-18}
	000-001	2.46 TO 3.13	2.5×10^{-2}	0.03×10^{-15}	7.5×10^{-19}

5.10 Vibrational Data for Ar - H_2O Collisions

A limited number of experiments were performed in the 5.67 to 7.45 μm wavelength interval using argon at 5.4 Km/sec colliding with H_2O as the target gas. The results of this study are reported in Table VIII. Using a radiative lifetime of 4.5×10^{-2} sec for the H_2O 000-010 vibrational-rotational transition gives an excitation cross section of about 2×10^{-18} cm^2.

Table VIII
CROSS SECTION FOR VIBRATIONAL EXCITATION OF H_2O IN COLLISIONS WITH ARGON AT 5.4 km/sec

FILTER	NO H_2O INJECTION	WITH H_2O INJECTION	SIGNAL DUE TO H_2O	$(\sigma_*/\tau)_{EXPT.}$	$\sigma_*(\Delta\lambda)$
microns	photons/sec	photons/sec	photons/sec	$cm^2\ sec^{-1}$	cm^2
5.67 TO 7.45	6.1×10^9	7.4×10^9	1.3×10^9	0.047×10^{-15}	2.1×10^{-18}

6. CONCLUSIONS

Measurements have been made of the spectral infrared radiative properties of H_2O, CO_2 and NH_3 molecules that have been involved in a single high-energy collision with N_2, O, or Argon. A pressure-driven reflected-shock tunnel was used to produce a supply of N_2 molecules at 5.8 Km/sec, a supply of O atoms at 4.3 Km/sec and a supply of Argon atoms at 5.4 Km/sec. Experimental values of excitation cross section/radiative lifetime (σ_* / τ) have been obtained for the 2.5 to 3.1 μm, 5.7 to 7.5 μm, 8.3 to 9.2 μm, 9.1 to 10.3 μm, 10.6 to 11.6 μm, 11.1 to 14 μm and 8.3 to 14 μm wavelength regions for N_2-H_2O collisions. For N_2-CO_2 collisions, measurements of σ_* / τ have been obtained in the wavelength regions 4.28 to 4.34 μm, 8.3 to 9.2 μm, 9.1 to 10.3 μm, 10.6 to 11.6 μm, and 8.3 to 14 μm. Measurements of σ_* / τ have also been obtained for N_2-NH_3 collisions in the wavelength intervals 8.3 to 9.2 μm, 10.6 to 11.6 μm and 8.3 to 14 μm. For O-H_2O collisions, measurements of σ_* / τ were performed in the wavelength interval 2.46 to 3.13 μm, 5.7 to 7.5 μm, and 11.1 to 14 μm. The experimental values of σ_* / τ are shown to compare favorably with theoretical calculations of the effective values of for radiation in the given wavelength intervals.

7. REFERENCES

1. Dunn, M. G., "Experimental Study of High-Enthalpy Shock-Tunnel Flow. Part I: Shock-Tube Flow and Nozzle Starting Time," AIAA Journal, Vol. 7, No. 8, Aug. 1969, pp. 1553-1560.

2. Dunn, M. G., "Experimental Study of High-Enthalpy Shock-Tunnel Flow. Part II: Nozzle-Flow Characteristics," AIAA Journal, Vol. 7, No. 9, Sept. 1969, pp. 1717-1724.

3. Laframboise, J. G., "Theory of Spherical and Cylindrical Langmuir Probes in a Collisionless Plasma at Rest," Rarefied Gas Dynamics, Vol. II, Academic Press, New York, 1965, pp. 22-44.

4. Rolling, R. E., Funai, A. I., and Grammer, J. R., "Investigation of the Effect of Surface Condition on the Radiant Properties of Metals," Air Force Materials Lab., Tech. Rept. 64-363, Nov. 1964.

5. Hudson, R. D., Infrared System Engineering, Wiley-Interscience, New York (1969).

6. Kieffer, L. J., "Compilation of Low Energy Electron Collision Cross Section Data Part I.," JILA Information Center Report No. 6, Univ. of Colorado, Boulder, Colorado (Jan. 1968).

7. Lampe, F. W., Franklin, J. L., and Field, F. N., "Cross Sections for Ionization by Electrons," J. Am. Chem. Soc., Vol. 79, pp. 6129-6132 (1957).

8. Kennan, J. H. and Kaye, J., Gas Tables, Wiley, New York (1945).

9. Handbook of Chemistry and Physics, 41st Edition, 1959-1960.

10. Kolb, C. E., Baum, H. R., and Tait, K. S., "Classical Calculations of H_2O Rotational Excitation in Energetic Atom-Molecule Collisions," J. Chem. Phys., Vol. 57, No. 9, Oct. 1972, pp. 3409-3416.

11. Maki, A., Tables of Rotational Energy Levels and Transitions for H_2O, National Bureau of Standards, Private Communication.

REFERENCES (Contd)

12. Benedict, W. S. and Plyler, E. K., "High-Resolution Spectra of Hydrocarbon Flames in the Infrared," in NBS Circular 523, U. S. Dept. of Commerce, March 1954, p. 64.

13. Schwartz, R. N., Slawsky, Z. I., and Herzfeld, K. F., "Calculation of Vibrational Relaxation Times in Gases," J. Chem. Phys., Vol. 20, p. 1591 (1952).

14. Rapp, D. and Sharp, T. E., "Vibrational Energy Transfer in Molecular Collisions Involving Large Transition Probabilities," J. Chem. Phys., Vol. 38, pp. 2641-2648 (1963).

15. Millikan, R. C. and White, D. R., "Systematics of Vibrational Relaxation," J. Chem. Phys., Vol. 39, pp. 3209-3213 (1963).

16. Simpson, C. J. S. M. and Chandler, T. R. D., A Shock Tube Study of Vibrational Relaxation in Pure CO_2 and Mixtures of CO_2 with the Inert Gases, Nitrogen, Deuterium and Hydrogen," Proc. Royal Soc., Series A, Vol. 317, pp. 265-277 (1970).

17. Buchwald, M. I. and Bauer, S. H., "Vibrational Relaxation in CO_2 with Selected Collision Partners. I. H_2O and D_2O," J. Phys. Chem., Vol. 76, pp. 3108-3115 (1972).

18. Brau, C. A., Lewis, P. L., Wu, P. K., and Young, L. A., "Plume Interference Assessment and Mitigation," AVCO Everett Research Laboratory (to be published).

19. Burch, D. E., Gryvnak, D. S., Singleton, E. B., France, W. L., and Williams, D., "Infrared Absorption by Carbon Dioxide, Water Vapor, and Minor Atmospheric Constituents," AFCRL-62-698, July 1962.

20. Penner, S. S. and Olfe, D. B., Radiation and Reentry, Academic Press, New York, 1968.

21. "Plume Interference Assessment and Mitigation," Calspan Rept. No. KC-5134-A-3, Section II. 2, Task II, Near-Field Analysis, AVCO Everett Research Laboratory, p. 12, Oct. 1972.

APPENDIX A

VIBRATIONAL DATA CORRELATION

The cross section for vibrational excitation as a function of impact velocity can be estimated by using collision theory in conjunction with measurements of vibrational relaxation. Collision theories yield that, for a collision between molecules which have an exponentially repulsive force, the probability of transition in a collision has the form

$$P_{10} = K_1 v^2 e^{-K_2/v} \tag{A-1}$$

and the cross section σ_* for this transition is

$$\sigma_* = \sigma_0 P_{10} = \sigma_0 K_1 v^2 e^{-K_2/v} \tag{A-2}$$

where σ_0 is the kinetic cross section. When the transition probability is averaged over a Boltzmann distribution of velocities, an expression for the vibrational relaxation time is obtained, of the form

$$p\tau = B e^{-AT^{-1/3}} \tag{A-3}$$

and this relation has considerable experimental confirmation. By following through the derivation (see, for example, Refs. 13 or 14) the constants in Eqs. (2) and (3) can be shown to be related by

$$K_2 = \left(\frac{2}{3} A\right)^{3/2} \sqrt{\frac{k}{\tilde{m}}} \tag{A-4}$$

and

$$\sigma_0 K_1 = \frac{9}{32\sqrt{2}} \frac{1}{N_0 T_0} \left(\frac{\tilde{m}}{k}\right)^{3/2} \frac{1}{B A^{3/2}} \tag{A-5}$$

The units of $p\tau$ have been taken as atmosphere sec. T is the temperature in °K, k is the Boltzmann constant, $\tilde{m}$ is the reduced mass of the colliding molecules, and N_o and T_o are the reference number density and temperature associated with the reference pressure of one atmosphere used in Eq. (A-3). Thus $N_o T_o = 8.067 \times 10^{21}$ (particles/cm^3) °K , and $\sqrt{\frac{k}{\tilde{m}}} = \frac{1}{\sqrt{\mu}}\ 9.117 \times 10^3$ deg$^{-1/2}$ cm/sec , where μ is the reduced molecular weight. Introducing these numbers, Eqs. (4) and (5) become

$$K_2 = 4962 \sqrt{\frac{A^3}{\mu}} \ cm/sec. \tag{A-6}$$

$$\sigma_o K_1 = 3.253 \times 10^{-35} \frac{1}{B} \left(\frac{\mu}{A}\right)^{3/2} sec^2 \tag{A-7}$$

and (2) is

$$\sigma_* = 3.253 \times 10^{-35} \frac{1}{B} \left(\frac{\mu}{A}\right)^{3/2} v^2 e^{-4962\sqrt{\frac{A^3}{\mu}}/v} \tag{A-8}$$

The constants A and B can be obtained from vibrational relaxation data, in cases where these are available. Otherwise, estimates can be obtained from the semi-empirical correlation relations of Millikan and White.[15] From a comparison of 13 sets of collision partners, they obtain

$$A = c\, \mu^{1/2}\, \theta^{4/3} \tag{A-9}$$

and

$$B = e^{-(0.015\, \mu^{1/4} A + 18.42)} \tag{A-10}$$

where θ is the characteristic temperature ω/k for the transition (in °K) and c is a number close to 1.16×10^{-3}. Thus if the Millikan and

White correlations are used, Eqs. (6) and (7) become

$$K_2 = 0.196\,\mu^{1/4}\,\theta^2 \tag{A-11}$$

$$\sigma_o K_1 = 8.228 \times 10^{-23}\,\mu^{3/4}\,\theta^{-2}\,e^{1.74\times10^{-5}\mu^{3/4}\theta^{4/3}} \tag{A-12}$$

and Eq. (2) is

$$\sigma_* = 8.228 \times 10^{-23}\,\mu^{3/4}\,\theta^{-2}\,e^{1.74\times10^{-5}\mu^{3/4}\theta^{4/3}}\,v^2\,e^{-(0.196\mu^{1/4}\theta^2)/v} \tag{A-13}$$

With μ in molecular weight units, θ in °K and v in cm/sec, the cross section σ_o is in cm^2. The value of P_v to be associated with vibrational excitation in Eq. (21) is then σ_* / σ_o

Values of the quantities in Eqs. (A-9) to (A-13) are given in Table A-I for the collisions of interest here.

Experimental results of Simpson and Chandler[16] (also see Ref. 17) give, for N_2-CO_2 vibrational relaxation, $A = 38°K^{-1/3}$, $B = 5 \times 10^{-8}$ atm sec. These values, when used in Eq. (A-8), give $\sigma_* = 4.0 \times 10^{-17}$ cm^2 for $v = 5.8 \times 10^5$ cm/sec.

Table A-1
MILLIKAN AND WHITE DIATOMIC CORRELATION APPLIED TO N_2 COLLISIONS WITH TRIATOMIC MOLECULES

COLLISION PARTNER	VIBRATIONAL TRANSITION	ENERGY	EQN. A-3		EQN. A-2		σ_* FOR $v_1 = 5.2$ km sec^{-1}	σ_* FOR $v_1 = 5.8$ km sec^{-1}
			A	B	$\sigma_o K_1$	K_2		
		cm^{-1}	$^oK^{-1/3}$	sec atm	cm^2	cm sec^{-1}	cm^2	cm^2
H_2O	000-010	1595	1.16×10^2	4.24×10^{-10}	2.24×10^{-27}	1.878×10^6	1.6×10^{-17}	3.0×10^{-17}
	000-001	2349	1.95×10^2	4.89×10^{-11}	8.83×10^{-27}	4.07×10^6	9.5×10^{-19}	2.7×10^{-18}
CO_2	000-010	672	4.59×10^1	2.47×10^{-9}	3.0×10^{-27}	3.727×10^5	4.0×10^{-16}	5.3×10^{-16}
	000-001	3755	4.55×10^2	9.20×10^{-15}	2.51×10^{-23}	1.16×10^7	1.4×10^{-21}	1.7×10^{-20}
NH_3	0000-0100	932	5.58×10^1	2.21×10^{-9}	1.21×10^{-27}	6.356×10^5	9.7×10^{-17}	1.4×10^{-16}

LIST OF SYMBOLS

a	y coordinate of the lower flat plate
A_d	area of infrared detector
A_{ij}	Einstein coefficient for spontaneous emission
b	distance of hot wire from mirror surface
b'	distance of virtual image from mirror surface
d	hot-wire diameter
d'	virtual-image diameter
D	dimension of (square) infrared detector
f	focal length of mirror
h	distance between the flat plates
I	blackbody spectral radiant emittance
L	length of the hot wire
N	spectral radiance of hot wire
n_1	number density of the incident stream
$n_2(y)$	number density of the target stream
P	maximum collision probability of collision for an incident stream particle in the target stream
P_R	probability of excitation of a given rotational state
P_v	probability of excitation of a given vibrational state
P_λ	power radiated by hot wire into detector in $\Delta\lambda$
R	spherical radius of mirror
T	hot-wire temperature
v_1	velocity of the incident stream
v_2	velocity of the target stream
v_*	velocity of the center of mass in an incident-target molecule collision
w	total flux of photons into detector (photons sec^{-1})
x	coordinate parallel to the incident stream
y	coordinate parallel to the axis of the target stream

LIST OF SYMBOLS (Contd)

z	coordinate at right angles to x and to y
δ	width of wire shadow on detector
ϵ_λ	spectral emittance of hot wire at temperature T
ξ	y / η
η	$v_2 / (v_1 n_1 \sigma_0)$
θ	apex angle of the target and field-of-view cones
$\bar{\theta}_y$	defined by Eq. (23)
λ	wavelength
$\Delta\lambda$	wavelength interval
σ_0	elastic collision cross section for the incident stream particle and the target gas
σ_{vR}	cross section for excitation to the v , R vibrational-rotational state
σ_*	collision cross section for a participating excited state
τ	lifetime of a participating excited state
$\phi_{*(y,z)}$	flux of excited states between target cone and field of view, (molecules cm^{-2} sec^{-1})
$\psi_2(y)$	total flux of target molecules (molecules sec^{-1})
$()_1$	pertaining to the incident stream
$()_2$	pertaining to the target stream
$()_*$	pertaining to a participating excited state